Quarterly Progress Report

June 1, 1995 to August 31, 1995

Visible Light Emitting Materials and Injection Devices

ONR/ARPA URI

Grant Number N00014-92-J-1895

Prepared by:

Paul H. Holloway
Department of Materials Science and Engineering
University of Florida
P.O. Box 116400
Gainesville, FL 32611
Ph: 904/392-6664; FAX: 904/392-4911
E-Mail: Internet-PHOLL@MSE.UFL.EDU

Participants:
University of Florida
Kevin Jones
Robert Park
Joeseph Simmons
Cammy Abernathy
Stephen Pearton
Dept. of Materials Science and Engineering
Timothy Anderson
Dept. of Chemical Engineering
Peter Zory
Dept. of Electrical Engineering
University of Colorado
Jacques Pankove
Dept. of Electrical Engineering
Columbia University
Gertrude Neumark
Dept. of Materials Science and Engineering
Oregon Graduate Institute of Science and Engineering
Reinhart Engelmann
Dept. of Electrical Engineering

19960501 090

REPORT DOCUMENTATION PAGE

FORM APPROVED
OMB No. 0704-0188

Public reporting burden for this collection of information is estimated to average 1 hour per response, including the time for reviewing instructions, searching existing data sources, gathering and maintaining the data needed and completing and reviewing the collection of information. Send comments regarding this burden estimate or any other aspect of the collection of information, including suggestions for reducing the burden to Washington Headquarters Services, Directorate for Information Operations and Reports, 1215 Jefferson Davis Highway, Suite 1204, Arlington, VA 22202-4302 and to the Office of Management and Budget, Paperwork Reduction Project (0704-0188), Washington, DC 20503

1. AGENCY USE ONLY (Leave blank)

2. REPORT DATE
Oct. 20, 1995

3. REPORT TYPE AND DATES COVERED
Interim Quarterly Progress Report for June 1, 1995 through August 31, 1995

4. TITLE AND SUBTITLE OF REPORT
Quarterly Progress Report on Visible Light-Emitting Materials and Injection Devices.

5. FUNDING NUMBERS
G:N-00014-92-J-1895

6. AUTHOR(S)
Paul H. Holloway

7. PERFORMING ORGANIZATION NAME(S) AND ADDRESS(ES)
University of Florida
Dept. of Materials Science and Engineering
P.O. Box 116400
Gainesville, FL 32611-6400

8. PERFORMING ORGANIZATION REPORT NUMBER:
N/A

9. SPONSORING/MONITORING AGENCY NAME(S) AND ADDRESS(ES)
Office of Naval Research
Dr. Y.-S. Park
800 North Quincy Street
Arlington, VA 22217-5000

10. SPONSORING/MONITORING AGENCY REPORT NUMBER:

11. SUPPLEMENTARY NOTES:

DISTRIBUTION STATEMENT E
Approved for public release
Distribution Unlimited

12a. DISTRIBUTION AVAILABILITY STATEMENT
Unlimited

12b. DISTRIBUTION CODE

13. ABSTRACT (Maximum 200 words)

A report is given on progress of our research into ZnSe-based and GaN-based materials and devices for light emitting diodes and diode lasers.

14. SUBJECT TERMS
Zinc Selenide
Gallium Nitride
Light Emitting Diodes
Diode Lasers

15. NUMBER OF PAGES:
42 + cover

16. PRICE CODE

17. SECURITY CLASSIFICATION OF REPORT:	18. SECURITY CLASSIFICATION OF THIS PAGE	19. SECURITY CLASSIFICATION OF ABSTRACT	20. LIMITATION OF ABSTRACT
Unclassified	Unclassified	Unclassified	Unlimited

DTIC QUALITY INSPECTED 1

GENERAL INSTRUCTIONS FOR COMPLETING SF 298

The Report Documentation Page (RDP) is used in announcing and cataloging reports. It is important that this information be consistent with the rest of the report, particularly the cover and title page. Instructions for filling in each block of the form follow. It is important to ***stay within the lines*** to meet ***optical scanning requirements.***

Block 1. Agency Use Only *(Leave blank)*.

Block 2. Report Date. Full publication date including day, month, and year, if available (e.g. 1 Jan 88). Must cite at least the year.

Block 3. Type of Report and Dates Covered. State whether report is interim, final, etc. If applicable, enter inclusive report dates (e.g. 10 Jun 87 - 30 Jun 88).

Block 4. Title and Subtitle. A title is taken from the part of the report that provides the most meaningful and complete information. When a report is prepared in more than one volume, repeat the primary title, add volume number, and include subtitle for the specific volume. On classified documents enter the title classification in parentheses.

Block 5. Funding Numbers. To include contract and grant numbers; may include program element number(s), project number(s), task number(s), and work unit number(s). Use the following labels:

C - Contract
G - Grant
PE - Program Element
PR - Project
TA - Task
WU - Work Unit Accession No.

Block 6. Author(s). Name(s) of person(s) responsible for writing the report, performing the research, or credited with the content of the report. If editor or compiler, this should follow the name(s).

Block 7. Performing Organization Name(s) and Address(es). Self-explanatory.

Block 8. Performing Organization Report Number. Enter the unique alphanumeric report number(s) assigned by the organization performing the report.

Block 9. Sponsoring/Monitoring Agency Name(s) and Address(es). Self-explanatory.

Block 10. Sponsoring/Monitoring Agency Report Number. *(If known)*

Block 11. Supplementary Notes. Enter information not included elsewhere such as: Prepared in cooperation with...; Trans. of...; To be published in.... When a report is revised, include a statement whether the new report supersedes or supplements the older report.

Block 12a. Distribution/Availability Statement. Denotes public availability or limitations. Cite any availability to the public. Enter additional limitations or special markings in all capitals (e.g. NOFORN, REL, ITAR).

DOD - See DoDD 5230.24, "Distribution Statements on Technical Documents."
DOE - See authorities.
NASA - See Handbook NHB 2200.2.
NTIS - Leave blank.

Block 12b. Distribution Code.

DOD - Leave blank.
DOE - Enter DOE distribution categories from the Standard Distribution for Unclassified Scientific and Technical Reports.
NASA - Leave blank.
NTIS - Leave blank.

Block 13. Abstract. Include a brief *(Maximum 200 words)* factual summary of the most significant information contained in the report.

Block 14. Subject Terms. Keywords or phrases identifying major subjects in the report.

Block 15. Number of Pages. Enter the total number of pages.

Block 16. Price Code. Enter appropriate price code *(NTIS only)*.

Blocks 17. - 19. Security Classifications. Self-explanatory. Enter U.S. Security Classification in accordance with U.S. Security Regulations (i.e., UNCLASSIFIED). If form contains classified information, stamp classification on the top and bottom of the page.

Block 20. Limitation of Abstract. This block must be completed to assign a limitation to the abstract. Enter either UL (unlimited) or SAR (same as report). An entry in this block is necessary if the abstract is to be limited. If blank, the abstract is assumed to be unlimited.

(I) Molecular Beam Epitaxy Growth of II-VI and III-Nitrides (Robert Park)

(a) Column III - Nitride Work

Exploratory work has been done concerning the MBE growth of In-containing nitrides and the results obtained so far are summarized below.

Initially InN thin films were grown on (100) silicon and (100) gallium arsenide substrates by rf plasma-molecular beam epitaxy using a variety of substrate temperatures, rf plasma powers, indium beam equivalent pressures (BEPs), and nitrogen background pressures. A variety of analytical tools were employed in an effort to find the most suitable growth parameters to provide the best crystal quality for InN grown on these substrates. The most extensive analysis concerned in-situ reflection high energy electron diffraction, but scanning electron microscopy, Auger electron spectroscopy, and high-resolution x-ray diffraction were also employed. Subsequently, $In_xGa_{1-x}N$ thin films were grown on epitaxial β-GaN buffer layers grown on β-SiC coated silicon.

The optimum growth conditions for InN growth on (100) silicon were found to be a substrate temperature of 480°C, an In BEP of 2×10^{-7} Torr, and a plasma power of 450W. Analysis indicated that a continuous film was formed under these conditions that adhered well to the substrate. Although a streaky RHEED pattern was observed, the presence of an additional phase was indicated in this case, suggesting the material was not purely zincblende. A narrow temperature regime (480°C - 450°C) was found for the growth of crystalline InN on (100) silicon.

In the case of InN growth on (100) GaAs, the optimum growth conditions were found to be a growth temperature around 520°C, an In BEP of 2×10^{-7} Torr, and a plasma power of 450W. The RHEED pattern observed indicated four-fold symmetry (suggestive of cubic material) and also the presence of twinning. High-resolution x-ray diffraction analysis suggested that the cubic phase was present. Similar RHEED patterns were observed for growth on (100) GaAs at lower temperatures (480°C) under similar growth conditions.

$In_xGa_{1-x}N$ films grown on epitaxial β-GaN buffer layers deposited on β-SiC/Si exhibited the highest degree of crystallinity, as evidenced by RHEED, when grown at a substrate temperature of 520°C, an In BEP of 2×10^{-7} Torr, a gallium BEP of 5×10^{-8} Torr, and a plasma power of 350W. The RHEED patterns observed under such conditions, although spotty, exhibited four-fold symmetry.

(b) Wide-Gap II-VI Work

Our work this quarter in the II-VI area has focused on the stacking fault issue. Our primary concerns in this regard are in-situ cleaning and growth initiation.

We have compared the S.F. density in ZnSe/GaAs films grown on thermally-cleaned surfaces versus H-atom treated surfaces and observed a dramatic reduction in the S.F. density in the case of the H-atom treatment process. We are currently optimizing the process with regard to the S.F. density in collaboration with 3M personnel who are supplying us with S.F. density data as measured

by etch-pit analysis.

We have also determined that the specific method of growth initiation can have a significant impact on the S.F. density and we are continuing to explore this issue.

(II) MOMBE Growth of III-N Materials (Cammy Abernathy)

Work this quarter has focused on optimizing the growth chemistry and resultant structural quality of the nitrides grown by MOMBE. The optimum group III chemistry has now been identified and a preliminary assessment of the utility of carbon-bonded nitrogen sources has been made. Using the best chemistry, the growth conditions have been optimized to produce material with structural quality equivalent to, or in the case of AlN and InN, superior to that reported for other techniques. In the next quarter, these optimized conditions will be used to grow doped GaN, both p- and n-type, using a variety of precursors.

The nitride films were grown by MOMBE in an INTEVAC Gas Source Gen II on 2" (0001) Al_2O_3 (AlN and GaN) and semi-insulating GaAs (InN). The AlN and GaN films on sapphire were preceded by a low temperature AlN buffer ($T_g \sim 425^{\circ}C$). A range of Group III precursors, common to those used in the deposition of other III-V materials, were employed. The sources included trimethylindium (TMIn), triethylindium (TEIn), and 7N In metal for the growth of InN. Trimethylamine alane (TMAA) and dimethylethylamine alane (DMEAA) were compared for the growth of AlN. GaN growth experiments were conducted with triethylgallium (TEGa) and tri-isobutylgallium (TIBGa). The primary Group V flux was provided by a Wavemat MPDR 610 ECR plasma source mounted directly in the growth chamber source flange. Experimentation with alternative gaseous nitrogen precursors was conducted using uncracked tertiarybutyl amine and tri-isobutyl amine.

Structural quality was quantified by x-ray rocking curve analysis of hexagonal (0002) reflections performed with a Philips MRD high-resolution 5-crystal diffractometer with a triple axis detector assembly. The surface morphology of the nitride films was characterized using tapping mode atomic force microscopy (AFM) with a Digital Instruments Nanoscope III and scanning electron microscopy (SEM) using a JEOL 35CF. Hall data was collected using the van der Pauw method utilizing RTA-alloyed In contacts ($T_a = 420^{\circ}C$). Optical absorption studies were performed using an OLIS/Cary 14 UV/VIS spectrophotometer.

The relative growth efficiencies of the nitrides are presented in Table II.1 as ratios of the Group III-nitride growth rates to the corresponding arsenide or phosphide growth rates. A significant increase in InN growth efficiency was observed when the less stable TEIn was substituted for TMIn. However, this trend was not consistent through the series of gallium precursors. Although TEGa exhibited a higher GaN growth efficiency than TMGa, there appears to be little advantage for utilizing the more weakly bound but more expensive and less volatile TIBGa. Growth rates obtained with the amine bonded alanes, DMEAA and TMAA, were

Table II.1. **Relative Growth Efficiencies of the Group III-Nitrides**

Source	$r_{nitr}/r_{arsenide,phosphide}$
Trimethylindium	41 %
Triethylindium	80 %
Trimethylamine alane	100 %
Dimethylethylamine alane	100 %
Trimethylgallium	12 %
Triethylgallium	56 %
Tri-isobutylgallium	23 %

comparable to these found for AlAs grown by MOMBE.

While good structural quality InN has been grown by MOMBE,[1] as evidenced by a X_{min} of 10% measured by ion channeling analysis, a significant concern for the low temperature growth of InN has been the high as-grown electron concentrations. It might be expected that carbon or some other impurity from the Group III source is responsible for this conductivity. However, the electrical properties of InN films grown at 525°C from TMIn, TEIn, and elemental In are similar with electron concentrations from 1.5 - 3.0 × 10^{20} cm^{-3} and mobilities from ~97 - 103 cm^2/V-s (Fig. II.1). This persistent background conductivity suggests that the Group III precursor is not directly responsible for the high electron concentrations. SIMS analysis shows high backgrounds of both carbon and oxygen even in samples grown from elemental In, thus incorporation of carbon donors may be responsible for the high n-type background. Steps are in progress to reduce the impurity concentrations arriving at the surface from the plasma source in order to further investigate the role of carbon in the In-containing materials.

This InN behavior contrasts with the more dramatic differences in the impurity backgrounds of AlN samples grown with TMAA and DMEAA. A substantial decrease in the C (from ~10^{21} cm^{-3} to ~10^{20} cm^{-3}) and O (from ~10^{20} cm^{-3} to ~10^{18} cm^{-3}) concentrations as determined by SIMS was observed in the DMEAA grown material. This drop in impurity levels is likely due to the absence of ether, which is required in the processing of the solid TMAA in the liquid DMEAA synthesis. Using DMEAA and ECR nitrogen plasma, we have demonstrated the growth of high quality AlN. AFM analysis of DMEAA/ECR N-derived AlN grown at 700°C indicated a RMS surface roughness of <8 Å which indicates a planarization of the substrate which showed an RMS roughness of ~ 14 Å. The good structural quality of these films was indicated by a 432 arc-sec Ω X-ray rocking curve FWHM.

A series of growth experiments were conducted to determine the optimum conditions for depositing epitaxial GaN by MOMBE. Structural quality, surface morphology and interband absorption were correlated to growth temperature, V/III ratio, and ECR plasma power. Growth temperature was found to have a dramatic impact on structural quality as determined by Ω scan x-ray rocking curve analysis. Fig. II.2 shows the FWHM for ~1 μm layers grown at substrate temperatures from 625°C to 925°C where a fourfold drop in peak width was observed. Growth rates varied little over this temperature range (4500 - 4000 Å/hour), suggesting neither Ga desorption nor Group V surface concentration were rate limiting factors.

A trend similar to that observed in structural quality was also observed in the UV/VIS optical absorption behavior. For samples grown at lower temperatures, a strong interband absorption tail was observed in the absorption spectra similar to the 2.3 - 2.7 eV feature observed in gas-source MBE and MOCVD material.[2,3] This interband absorption feature decreased monotonically with increasing temperature. Attenuation coefficients for films grown at 10 sccm N_2 flow, 200 W ECR power, and 625°C and 925°C are shown

Fig. II.1. Van der Pauw hall data taken from InN samples grown with tri-ethylindium, trimethylindium, and elemental indium.

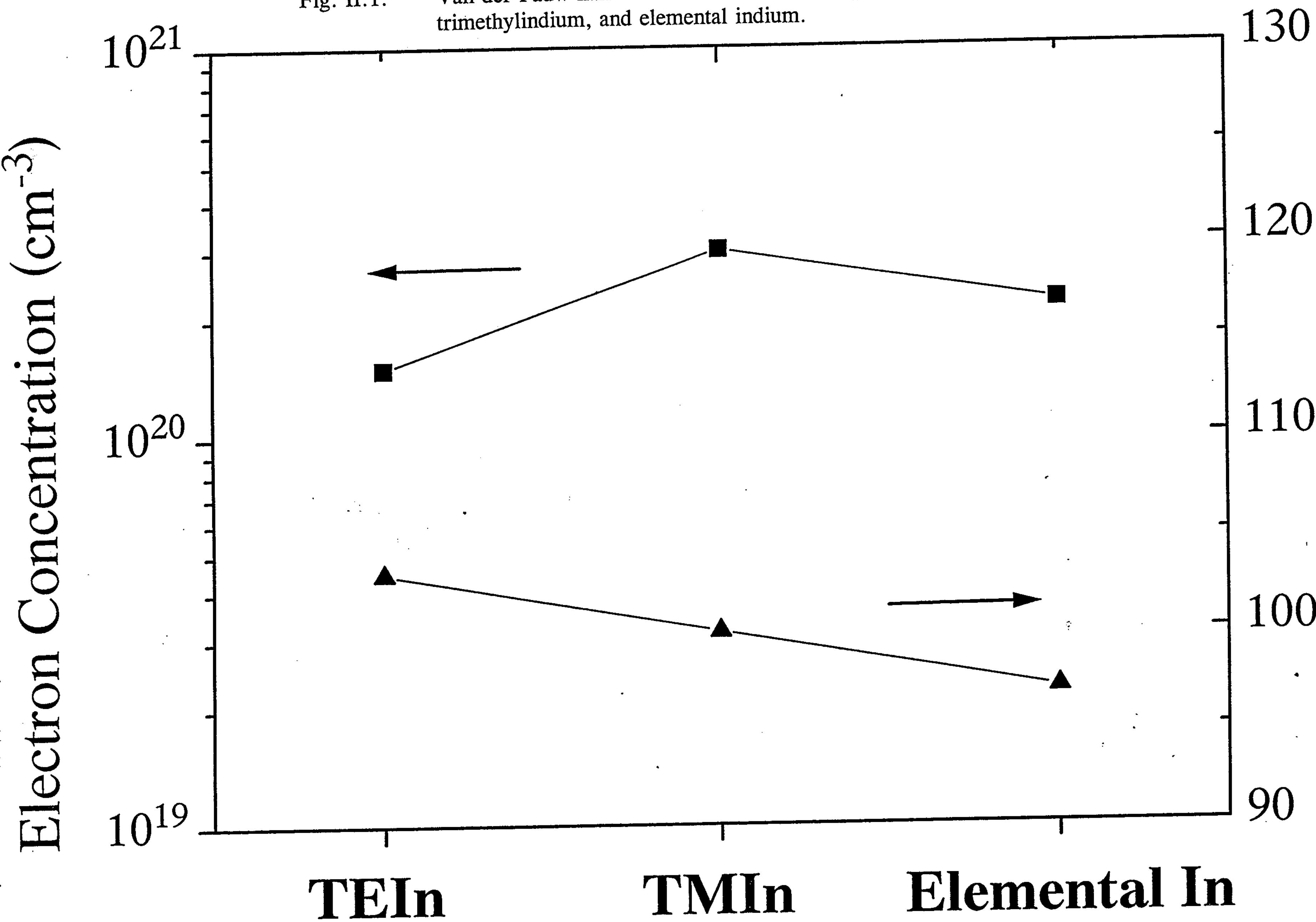

Fig. II.2. Ω scan x-ray rocking curve widths as a function of growth temperature for TEGa/ECR N derived GaN.

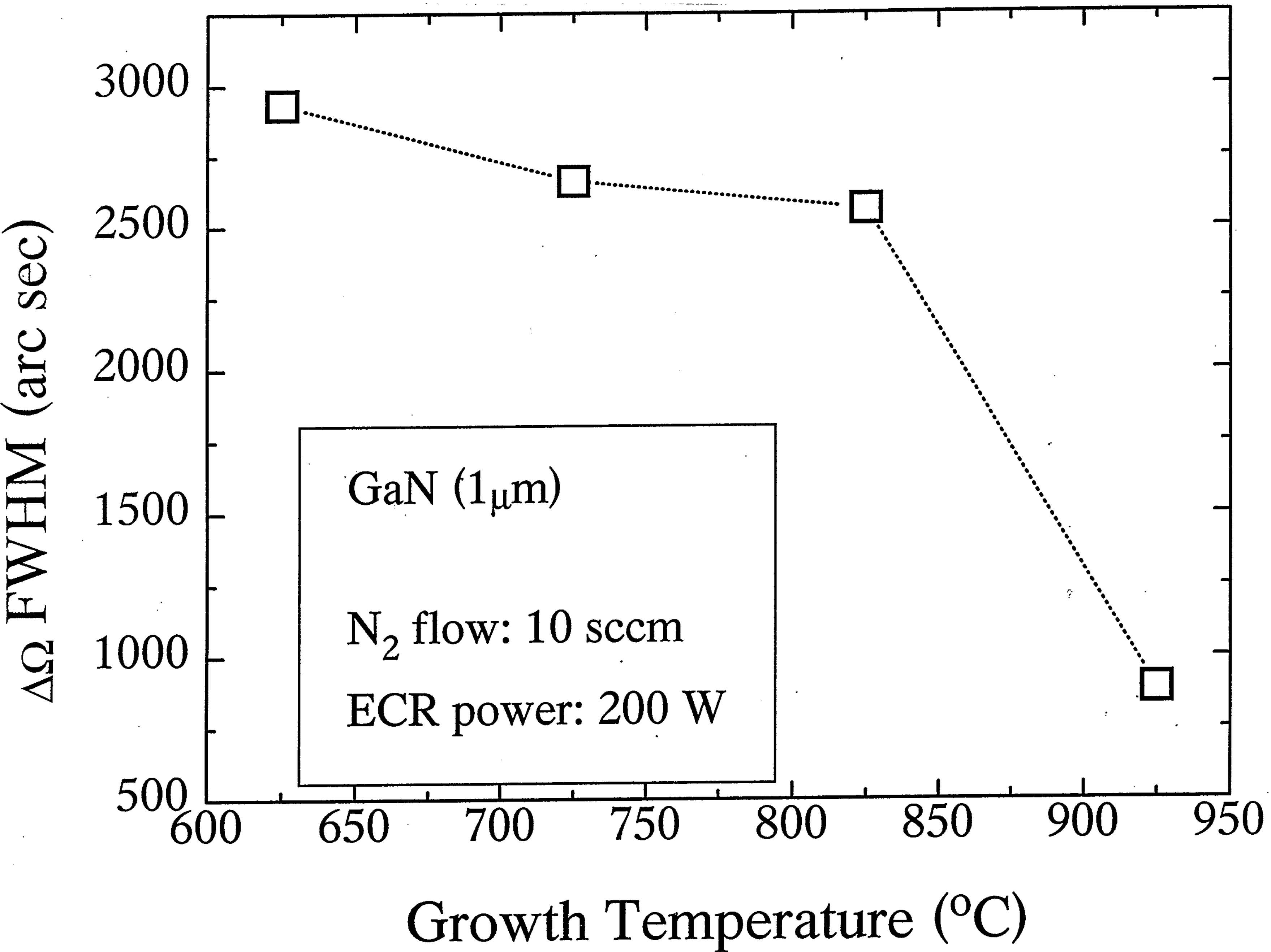

in Fig. II.3. Numerical fitting of the temperature dependence of the absorption coefficient measured at 2.9 eV indicated that the removal or deactivation of the optically active center was responsible for this interband absorption followed by thermal activation energy of ~110 meV.

Surface roughness as quantified by AFM also showed a significant temperature dependence as shown in Fig. II.4 where a peak in RMS surface roughness was observed in samples deposited at 825°C. The reductions in roughness at higher temperatures correspond with the improvements in the structural quality observed in the x-ray data. This further supports the trend toward high quality epitaxial growth at elevated temperatures. The planarization at low substrate temperatures may represent a planar growth mode approaching the regime exploited in low temperature buffer layers.

Reduction of the N_2 flow into the ECR plasma source, effectively lowering the V/III ratio, also had a substantial impact on film properties. Surface morphology was affected considerably as shown in the 10 KX SEM micrographs in Fig. II.5. Not only did the RMS roughness values improve by approximately 45%, there was a marked difference in the nature of the surface features for GaN grown using 10 sccm versus that using a 5 sccm N_2 flow. X-ray FWHM (Ω scan) also improved for these films from 755 arc·seconds (10 sccm) to 573 arc·seconds (5 sccm). As well, a decrease in interband optical absorption was observed in films grown under 5 sccm of N_2 flow versus those grown at 10 sccm (Fig. II.4). These results clearly indicate that the growth rates used in this technique are not limited by the rate of arrival of the nitrogen to the growth front.

Varying the ECR power had a less consistent effect on film properties. GaN films grown with an ECR power of 150 W (T_g = 725°C, N_2 flow 10 sccm) exhibited an AFM RMS surface roughness of 16.6 nm which is approximately 20% less than that of films grown under 200 W ECR power. However, below band edge absorption was virtually unaffected by the same change in ECR power. Also, the structural quality of films, as determined by Ω scan X-ray FWHM, deteriorated substantially from ~0.7° for films grown under 200 W to >>1° in films grown with 150 W ECR power. These results suggest that the very sensitive dependence of film qualities on ECR power reported for MBE[4] is not observed in MOMBE growth of GaN. In addition, the presence of higher energy nitrogen radicals under higher ECR powers do not seem to degrade optical or structural properties. It should be noted however, that increasing the growth rate, by increasing the TEG flow, does typically lead to poorer structural quality.

This optimization study of TEGa/ECR N GaN demonstrates that high quality material can be grown by MOMBE. However, growth rates for the practical fabrication of thick layers still remain an issue for UHV techniques, particularly if thick layers are needed to maximize structural quality near the active device layers. Fig. II.6 shows the high resolution x-ray diffractions rocking curves of the (0002) GaN reflection for a 4 μm layer grown at ~ 5000 Å/hr using the optimum conditions described above. High resolution 5 crystal x-ray analysis with the use of a triple axis allows the

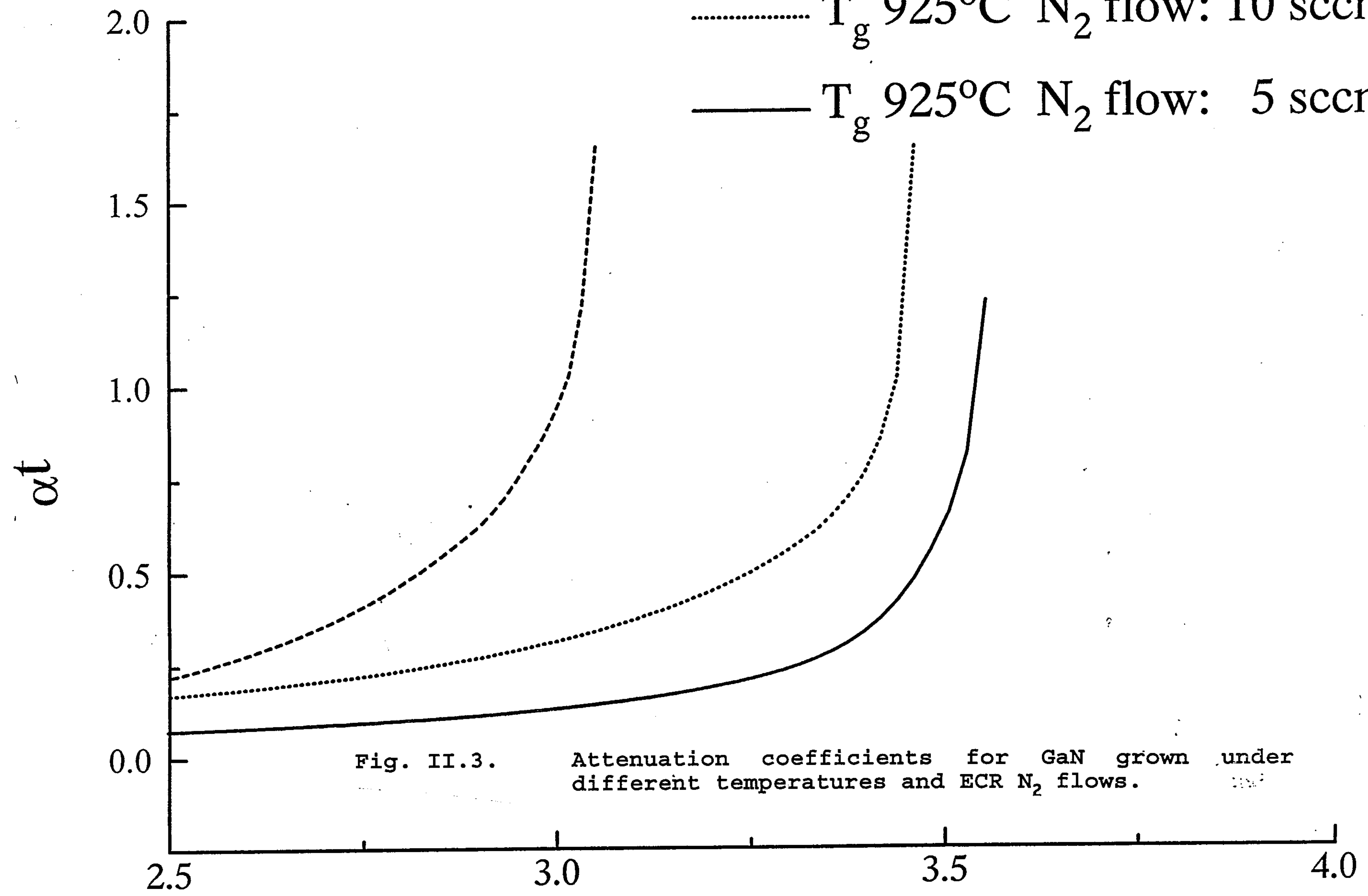

Fig. II.3. Attenuation coefficients for GaN grown under different temperatures and ECR N_2 flows.

Fig. II.4. AFM surface roughness of TEGa/ECR N GaN as a function of growth temperature.

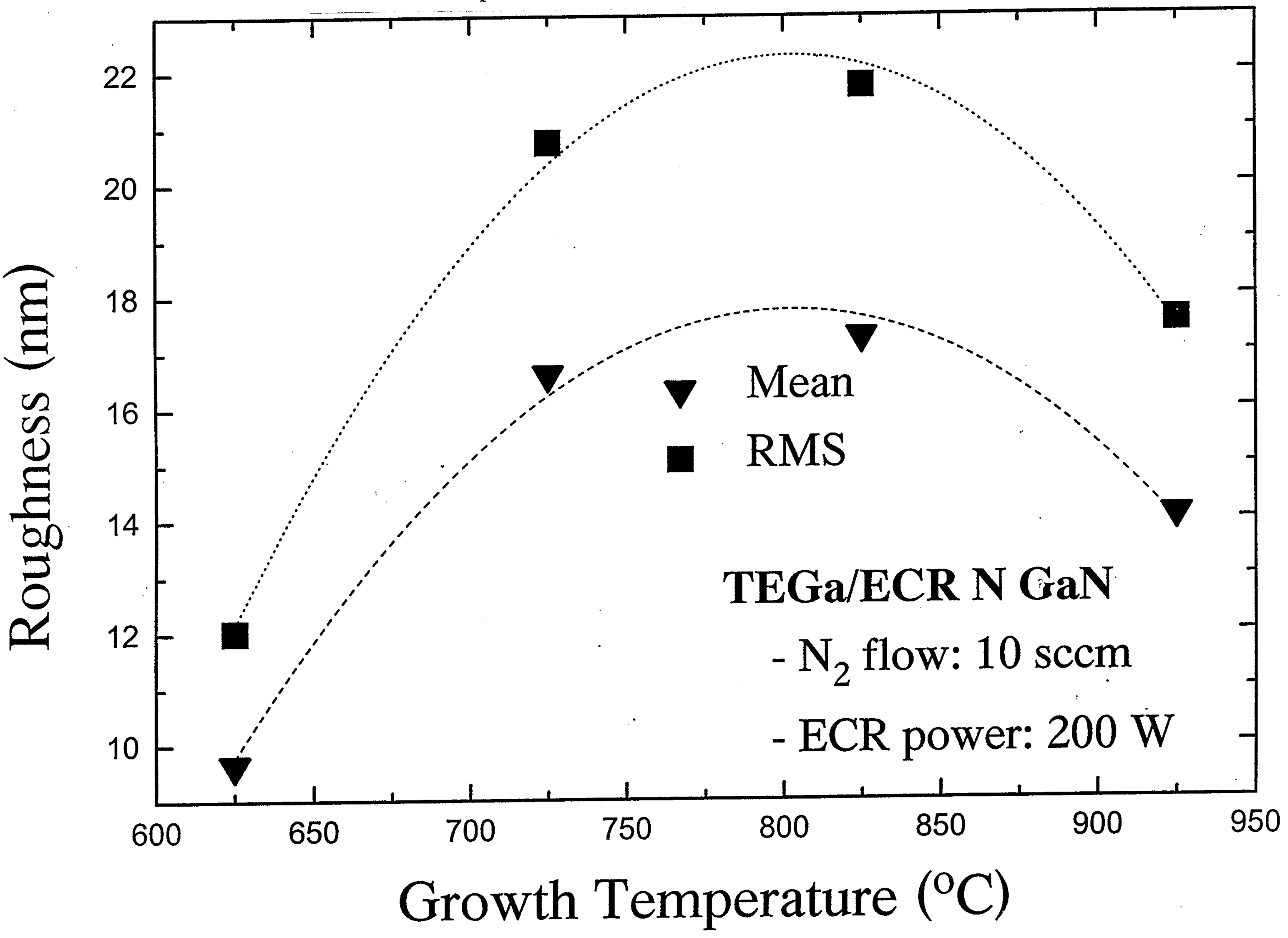

Fig. II.5a & b. 10 KX SEM micrographs of GaN surfaces grown with 10 sccm and 5 sccm of N_2 flow into the ECR source.

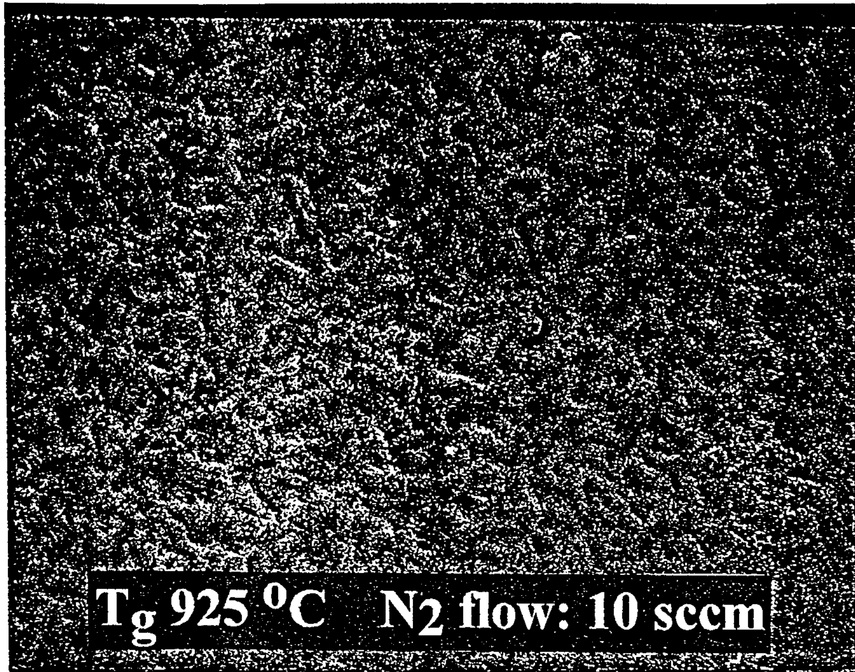

(a)

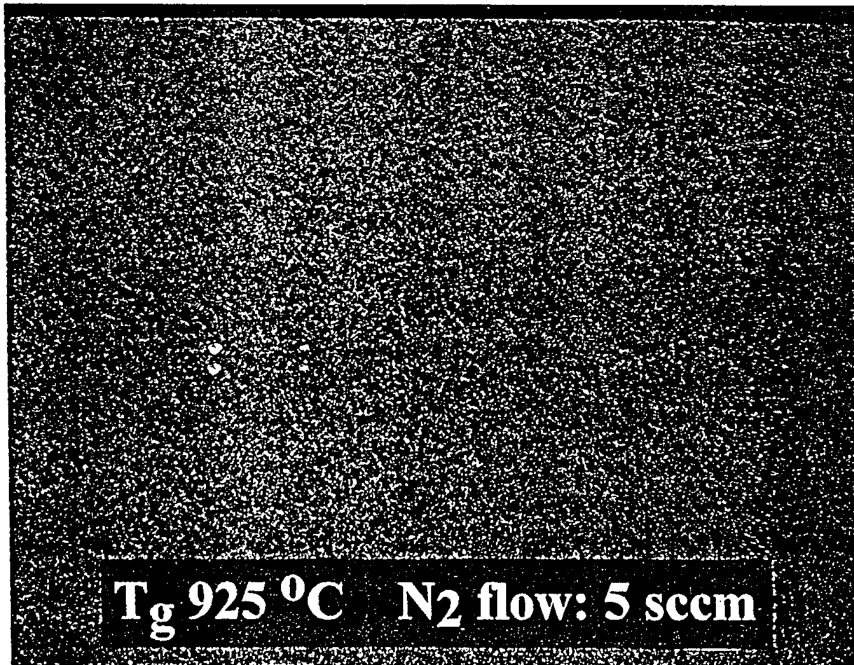

(b)

Fig. II.6. Ω and $\Omega/2\Theta$ high resolution x-ray rocking curves from a 4 μm thick GaN film grown at a rate of 5000 Å/hr.

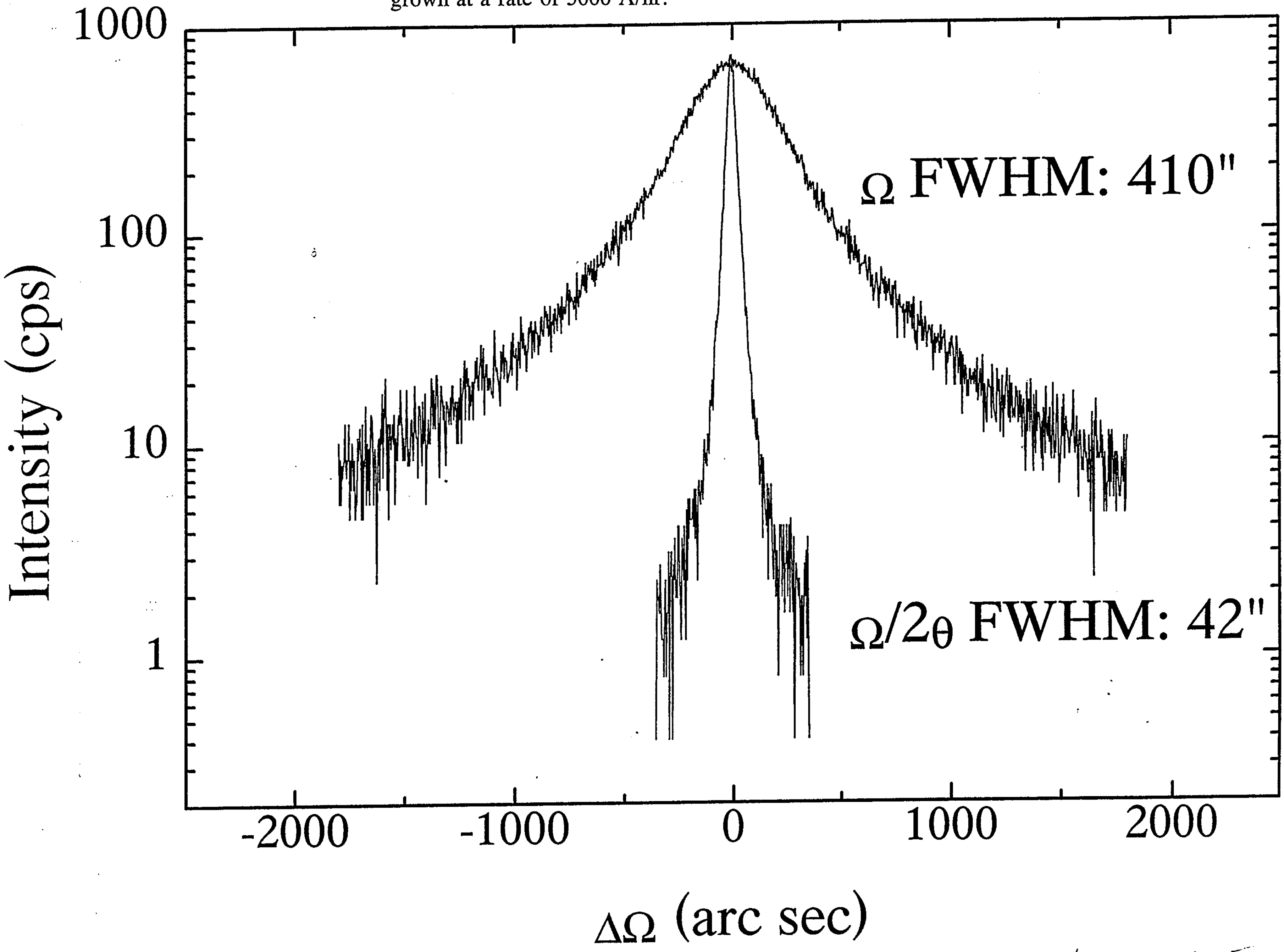

precise separation of peak broadening effects. Fixing the detector angle (2θ) and varying the incident angle (Ω) maps the shape of the Bragg reflection. The width of this peak depends directly on sample mosaicity, microtilts and structural perturbations which reflect the structural quality of the epitaxial layer. Operating in the symmetric mode, where both the incidence angle Ω (or θ) and the detector angle 2θ are varied, produces an x-ray curve for which the FWHM primarily reflects the variation in lattice constant. An Ω scan FWHM of 6.8 arc·minutes and an Ω/2θ FWHM of 42 arc·secs was measured for the 4 μm GaN sample. This shows an improvement in FWHM as compared to peak widths from 1 μm samples grown under the same conditions where we measured an Ω width of 9.6 arc·minutes and an Ω/2θ FWHM of 48 arc·secs. This thickness dependence in FWHM follows a general trend that can be seen in Fig. II.7 where some of the best FWHM values reported in the literature[5,4,5,6,7,8], GaN on Al_2O_3 have been plotted as a function of film thickness. In terms of structural quality, the MOMBE grown samples from this study are quite competitive with materials grown by other techniques, and the Ω and Ω/2θ FWHM values generally follow the trend of decreasing width with increasing film thickness.

Although we were able to dramatically improve the quality of ECR plasma-derived GaN by varying the growth parameters, the growth rate varied little. This is particularly interesting in the case of lowering the N_2 flow, especially at high temperatures where Group V desorption would be accelerated. Decoupling of growth from the effective V/III ratio suggests that the abundance of reactive nitrogen species at the growth surface does not limit the growth rate of high quality material. This supports the premise that epitaxial growth may be controlled by the surface mobility of nitrogen species. If the nitrogen surface mobility can be increased by weakly binding the N to a ligand such as iso-butyl or t-butyl, it may be possible to increase the growth rate without degrading the crystallinity. To investigate this, experimentation with two gaseous nitrogen precursors, tertiarybutyl amine and tri-isobutyl amine, was conducted. Unfortunately, though we were able to grow AlN from both precursors, we were unable to grow GaN under any growth conditions, presumably due to poor pyrolysis of the nitrogen precursor. In addition, the AlN films deposited from these sources possessed high impurity backgrounds and poor structural and optical properties. Thus it does not appear that carbon-bonded nitrogen sources will be suitable alternatives to plasma.

In summary, we have demonstrated the high quality growth of InN, AlN and GaN by MOMBE. Although TEIn was the most efficient source for InN growth, there was little variation in electrical properties for films grown with TEIn, TMIn, or elemental In. However, the quality of AlN films were quite different for DMEAA and TMAA precursors. A substantial reduction in C and O backgrounds was observed in AlN grown with the liquid DMEAA. TEGa proved to be the best precursor for GaN and the optimization experiments conducted in this work determined that high growth temperatures (925°C), lower V/III ratio (5 sccm N_2) and 200 W ECR power produced the highest quality films in terms of structural

Fig. II.7. A comparison of x-ray data for GaN grown on Al_2O_3 reported by a number of groups.

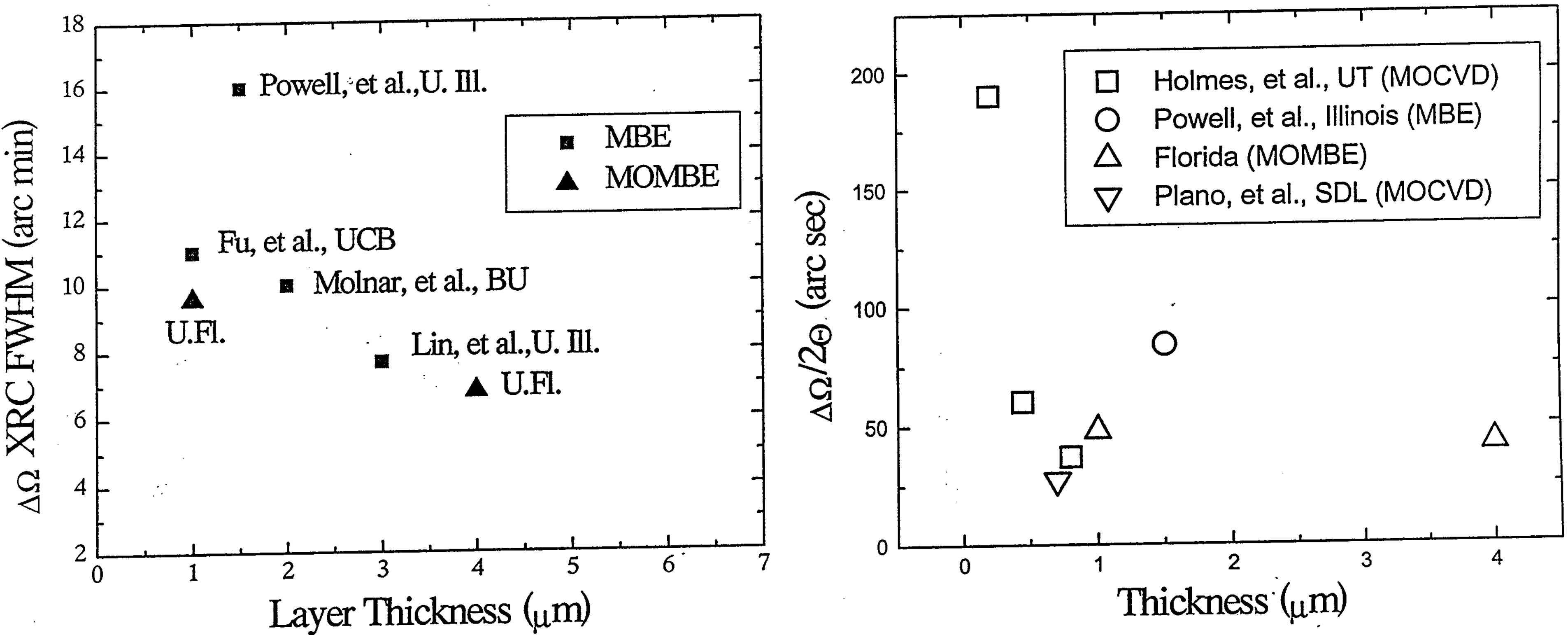

quality, surface morphology and minimized interband absorption. The preliminary experiments with the alternative nitrogen sources suggest that a non-carbon bonded nitrogen precursor may be required for high quality growth.

(III) Processing of Nitrides (Steve Pearton)

Diffusion of Implanted Dopants in GaN

Both Si and Mg were implanted into GaN/Al_2O_3 at a dose of 10^{14} cm^{-2} and an energy of 100 keV, and subsequently annealed in an RTA system under N_2 at temperatures up to 1150°C. Fig. III.1 shows SIMS profiles of the Si before and after an anneal at 1150°C; there is no discernable motion of the dopant under these conditions. Using a simple $(Dt)^{0.5}$ calculation, we can estimate that the diffusivity of Si in GaN is < 7×10^{-13} cm^{-2} at 1150°C. For Mg, Fig. III.2 shows a redistribution of ~500Å after an 1150°C anneal. This corresponds to a diffusivity of ~2×10^{-13} cm^{-2}, or approximately 4 orders of magnitude lower than in GaAs. These results confirm the extremely good thermal stability of dopants in GaN,and also indicate that implantation is the only feasible ex-situ method of impurity introduction in GaN. We have recently achieved implant activation in this material by annealing at temperatures of 1050°C, and have shown that the GaN surface retains its stoichiometry and structural stability under these conditions.

Ohmic Contacts on n^+ GaN

Sputtered W was deposited onto n^+GaN (~10^{18} cm^{-3}) and subsequently annealed at temperatures up to 1000°C. The contacts were examined by TLM measurements, RBS,TEM,AES and XRD. We found that there was minimal interaction of the GaN with W up to 900°C. At 1000°C, there was a reaction between the metal and the semiconductor, producing an interfacial layer containing WN_x phases approximately 50 Å thick. However there was little change in the electrical quality of the contacts. A minimum specific contact resistance of 10^{-5} ohm-cm^{-2} was achieved after annealing at ~700°C. We have performed similar experiments on InGaN and achieved R_c values of 8×10^{-6} ohm-cm^{-2}.

(IV) Ohmic Contact Formation (Paul Holloway)

a) degradation of Au/Pd/ZnTe/ZnSe ohmic contacts to p-ZnSe

Samples have been degraded using three types of electrical probes to make contact with the Au/Pd/ZnTe/ZnSe ohmic contacts. The three different probes were used to identify the effects of probe composition and size on contact degradation. The electrical probes include a copper (Cu) probe, a gold (Au) probe, and silver paint. Both the Cu and Au had a tip radius of ~1 mm and inspection of the samples following degradation indicate that the contact area between the probe and Au layer was ~ 600 μm^2. The silver paint contacts were much larger and had a contact area of ~ 3 mm^2.

Using the Cu and Au probes, samples were degraded at 30 A/cm^2

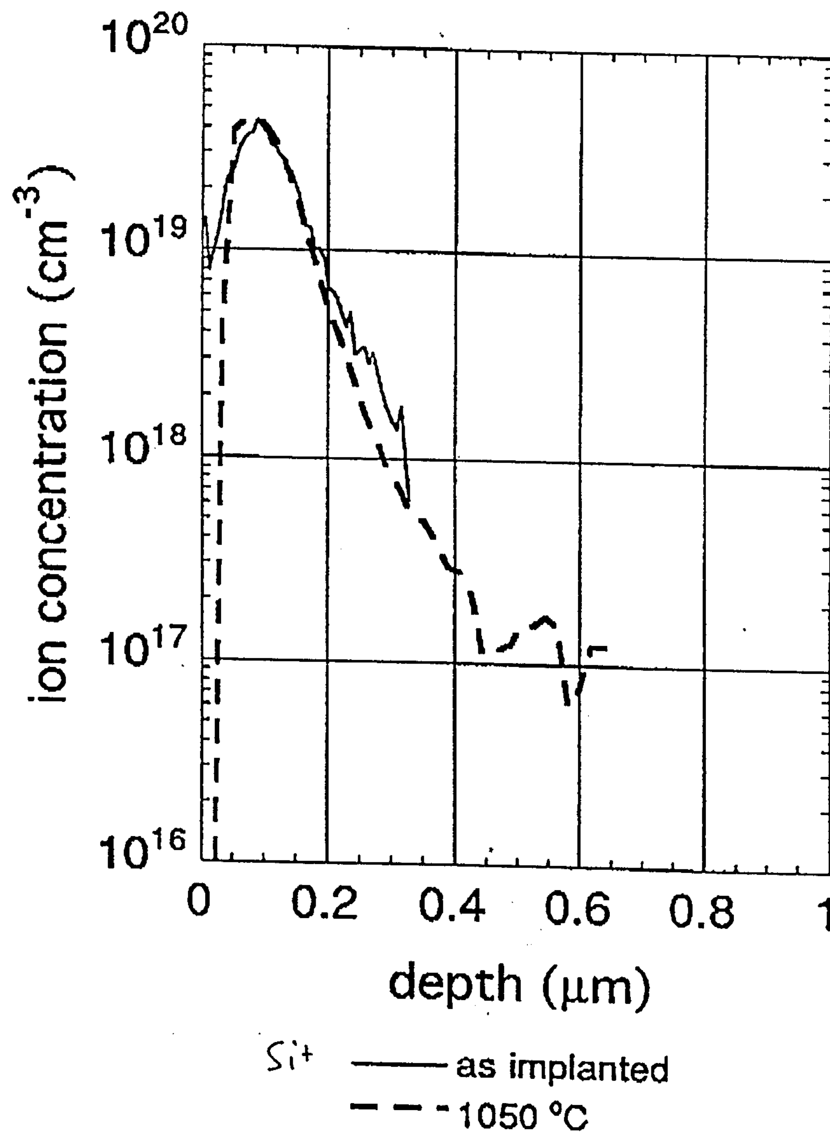

Fig. III.1.

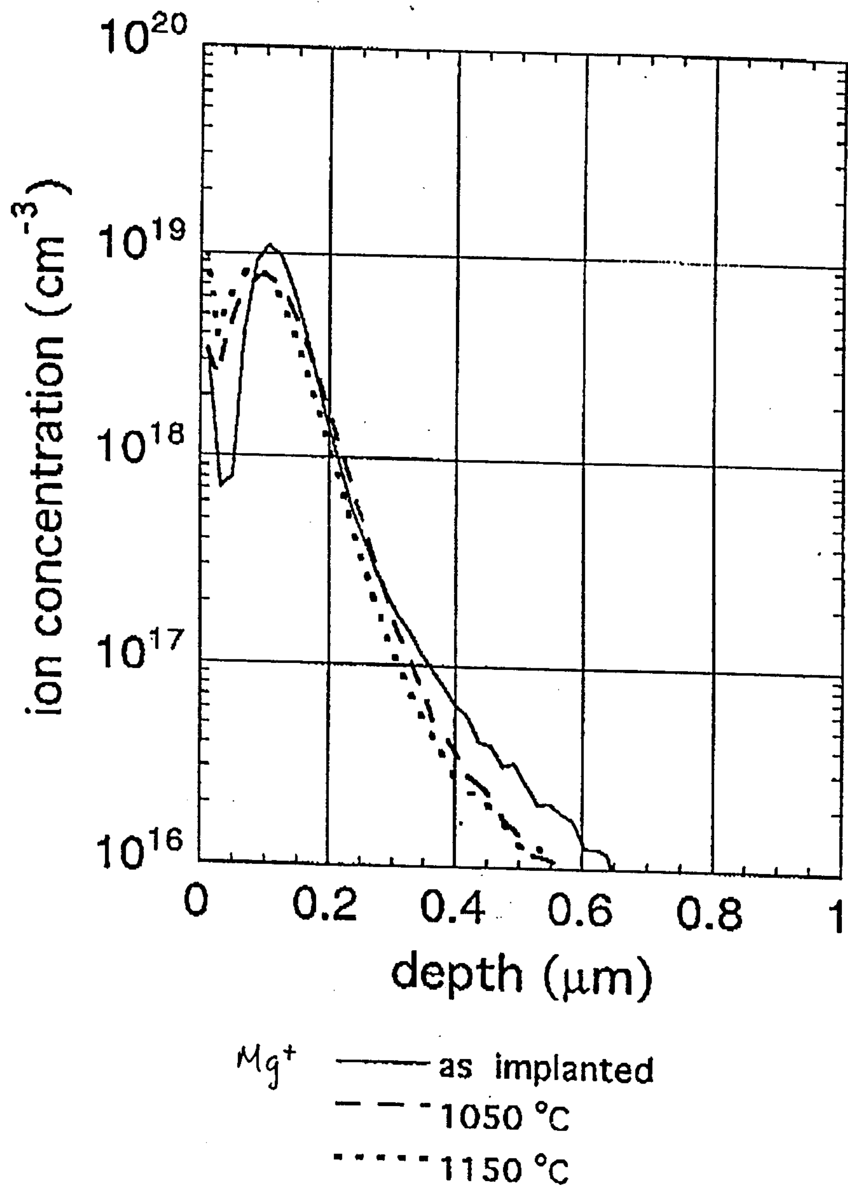

Fig. III.2.

for 6 to 90 minutes. During degradation, the samples were mounted on a Cu heat sink which reached temperatures of ~ 110 °C. Analytical results from the samples degraded using the Cu probe show that Cu alloys with the Au /Pd layer of the ohmic contact. In addition, large amounts of Cu are found to permeate through the ZnTe and ZnSe layers to the ZnSe/GaAs interface. This resulted in the formation of a Cu rich region at the ZnSe/GaAs interface which was up to 2 μm thick. The Cu is believed to have rapidly diffused through the ZnSe region along dislocations which acted as diffusion pipes. As reported earlier, raised rectangular (2 to 5 μm in length) features were observed on the surface of the samples following degradation. These features were found to form for both Cu and Au probes and surround the point at which the probe contacts the sample surface. Removal of the metal overlayers by wet chemical etching revealed elongated cracks along the edges of the rectangular features. Auger depth profiles from contacts degraded using both Cu and Au probes showed that in both cases, Zn, Te and Se diffused to the surface of the samples. On the sample surface, Zn reacted with atmospheric gases/contaminants to form ZnO and/or $ZnCO_3$.

Silver paint contacts were used to degrade samples at 10 A/cm^2 for up to 120 hours at ~110°C. For these samples, Zn was again found to diffuse to the samples surface, but no changes in surface morphology were observed. Analytical results indicate that a compound formed between the Pd and ZnTe layers in the contact structure. The larger contact area was found to significantly improve contact lifetime.

To identify the temperatures required to produce the reactions observed during the electrical degradation of the contacts, Auger depth profiles were obtained from samples heat treated at 200, 300, and 400°C. These samples showed that the Pd/ZnTe compound formed at 200 and 300°C but were unstable at higher temperatures. At 400°C, Zn, Te and Se were observed to diffuse to the samples surface. These results indicate that localized heating occurred when the Cu and Au probes were used. The resulting temperatures appear to be greater than observed during the operation of ZnSe-based laser diodes, based on lack of a spectral shift. These temperature discrepancies and the extent of localized heating are currently being investigated in our study.

b) <u>Ohmic Contacts to p-ZnTe</u>

Studies of the formation of ohmic contacts to p-ZnTe using Au metallizations (1100Å) continued. The films were analyzed by current-voltage (I-V) measurements as-deposited and following post deposition annealing. The as-deposited contacts were rectifying, but heating for 15 minutes at T≥150° resulted in ohmic behavior. Resistance increases were observed for longer times at all temperatures measured with large increases occurring following a 350°C heat treatment. Auger electron spectroscopy (AES) and secondary ion mass spectrometry (SIMS) profiles were used to show that the ohmic behavior was attributed to diffusion of acceptor-doping of Au in the p-ZnTe layer, which led to increased conductivity through the near surface layer at 250°C. Diffusion

was extensive and was coupled with compound formation at 350°C leading to degradation of the contact properties.

This work was presented under the title "Electrical Contacts to p-ZnTe" J.T. Trexler, J.J. Fijol, L.C. Calhoun, R.M. Park, and P.H. Holloway at the Seventh International Conference on II-VI Compounds and Devices, Edinburgh, UK, August 13-18, 1995, and will be published in the conference proceedings.

c) Ohmic Contacts to p-GaN

Ohmic contact metallizations of Au and Au/Ni to p-GaN were investigated using I-V measurements, AES, and SIMS. The Au contacts were DC magnetron sputter deposited while the contacts with a 500Å interfacial Ni layer were electron beam evaporated. All contacts were rectifying as deposited with the Au contacts remaining rectifying up to T=600°C for 30 minutes. The Au/Ni contacts exhibited nearly linear I-V data after a 400°C anneal. AES and SIMS showed no penetration of the Au into the GaN lattice upon annealing, but evidence of Ni diffusion into the p-GaN matrix and also throughout the Au contact layer. It is believed that the mechanism of Ni degenerating the GaN matrix provides the opportunity for doping of the near surface region of the p-GaN, leading to increased conduction.

(V) Degradation Study of II-VI LEDs (Kevin Jones)

The [100] dark line defects(DLD) observed using electroluminescence microscopy (shown in the previous report) during II-VI LED operation was further investigated. The very early stages of DLD evolution was of main interest in order to see whether pre-existing defects play a role in DLD development. LEDs were fabricated using a large Au contact area from the same structure of ZnCdSe QW/ZnSSe/ZnMgSSe/GaAs as reported earlier. LEDs were degraded until the final output power decreased to 80%, 75% and 50%, respectively, of the initial output power. DLDs were observable in the electroluminescence microscope after each of these three stages of degradation. However, these DLDs were not observed in the TEM. The reason might be that although some point defects were generated during degradation, they had not formed any extended defects that were observable in the TEM. Also, the spacing between these DLDs may be too large to confirm their existence at the high magnifications used in a TEM. The pictures of DLDs observed in TEM and shown in the previous report were taken from the sample which was degraded down to 10% of the initial output power wherein the DLDs are closely spaced. In order to investigate any strain change in the quantum well after degradation, low temperature photoluminescence was carried out. The temperature of the PL chamber cooled by liquid He was about 23K. The results are shown in Fig. V.1. Both samples were degraded down to 50 % of the initial output power. Sample #901 has a ZnCdSe QW/ZnSSe/GaAs structure and sample #937 consists of a ZnCdSe QW/ZnSSe/ZnMgSSe/GaAs structure. If the strain in the ZnCdSe quantum well was relaxed during degradation, the PL peak from the

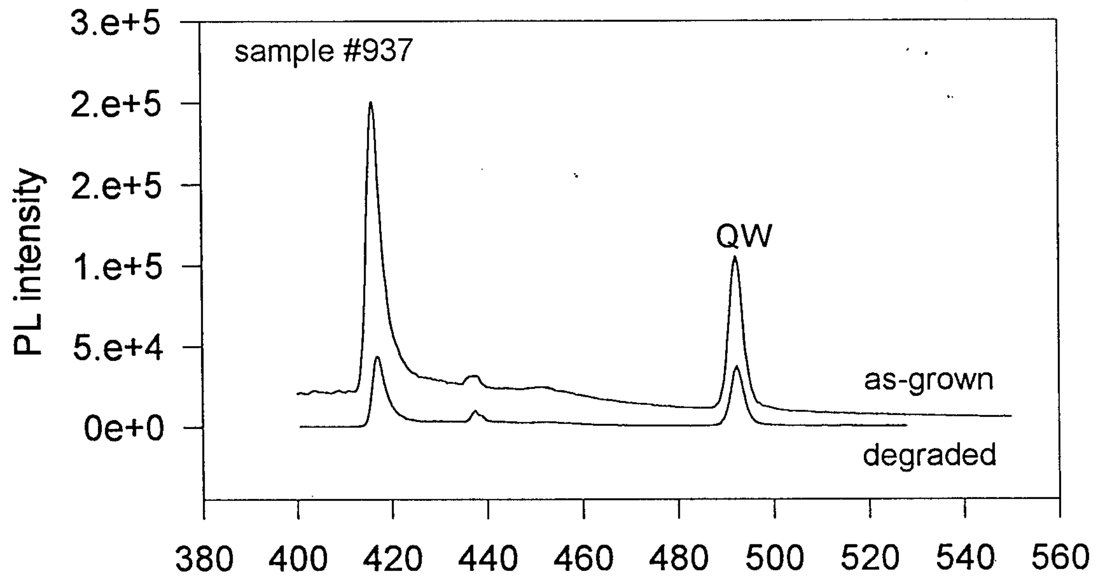

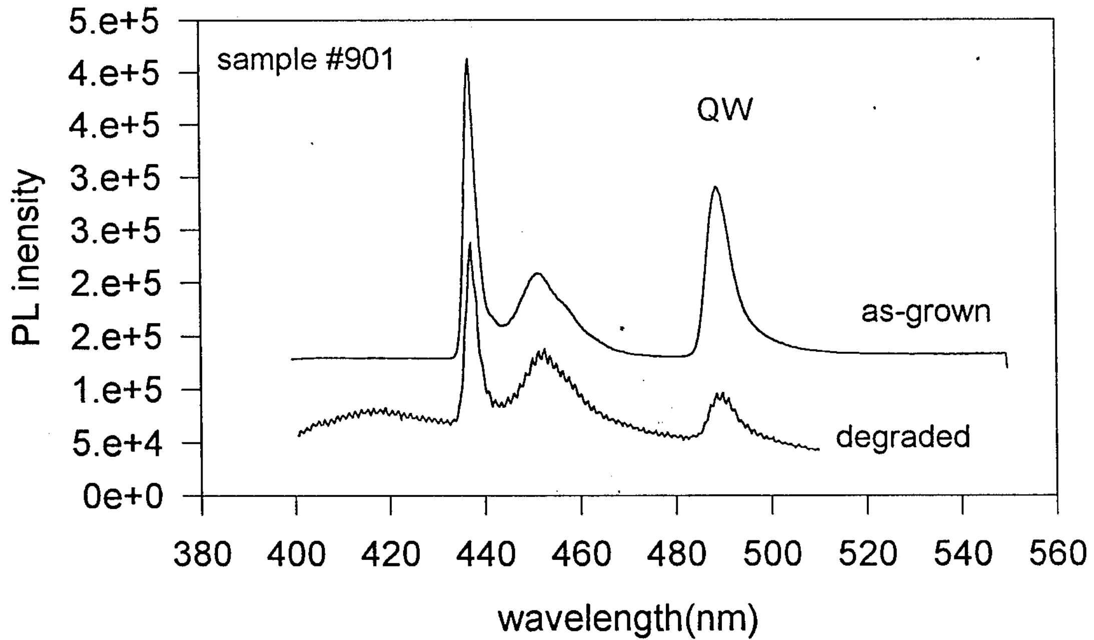

Fig. V.1.

QW should shift to a higher wavelength. The amount of bandgap difference between the strained and fully relaxed state of the quantum well in these structures is around 30 meV. However the PL peaks from the quantum well remained at about the same position which implies that the strain in the quantum well was not relaxed during the rapid degradation of II-VI light emitters.

(VI) MOCVD Growth of GaN Thin Films (Tim Anderson)

The effort in the growth of column III nitrides includes the use of two chemistries: low temperature conventional MOCVD and a merged metalorganic-hydride VPE chemistry. Efforts at growing high quality GaN at lower temperature (<900°C) have been motivated by the difficulty of incorporating In due to its relatively high elemental vapor pressure. The growth conditions have been optimized using TEGa and NH_3 to achieve high structural quality GaN on sapphire substrates, yielding a FWHM value of 49 arcsec (omega/2theta) for films grown at 850°C. During the past period, a new substrate source became available that provides nearly lattice-matched conditions and our efforts have focused on testing the possibility of this substrate.

Dr. Bruce H. T. Chai of the University of Central Florida contacted us concerning his production of two GaN lattice matched substrates, namely $LiGaO_2$ and $LiAlO_2$ (a_{GaN} = 3.189 Å, a_{LiGaO2} = 3.186 Å, and a_{LiAlO2} = 3.134 Å). These materials have a crystal structure similar to ZnO if one considers ZnO of the stoichiometry $ZnZnO_2$, with Li replacing one sublattice and Al or Ga on the other. In typical GaN film growth on sapphire and 6H-SiC substrates, a nitridation period followed by the growth of a low temperature buffer layer are crucial for growth of high quality GaN films. With these new lattice-matched substrates, it should be possible to grow GaN of higher quality without the use of a buffer layer.

A series of etching tests were performed on these substrates to determine an adequate pregrowth etching solution. A cold $H_2SO_4:H_3PO_4$ solution was identified to be best for substrate preparation. This etching method revealed pits on both substrates that are presumably due to stacking faults. The estimated density was on the order of 10^4 to 10^5 cm^{-2}. The etch rate was on the order of 0.2 μm/hr and other acid etches (HF, HCl,...) gave poor surface morphologies.

Three growth temperatures 650, 700 and 750°C were investigated for the growth of epitaxial GaN on these substrates. A color change was noticed when using the $LiGaO_2$ substrate, while no effect was observed when using the $LiAlO_2$ material. This phenomena can probably be attributed to the reaction of H_2 at high temperature to reduce Ga to the +1 oxidation state (Ga^2O) at the interface.

The quality of the GaN layers on $LiGaO_2$ appear to be very good at a growth temperature of 650°C. Under a Nomarski contrast microscope, the epilayer surface morphology was spectral. The growth rate was on the order of 0.3 μm/hr which is somewhat lower than observed with the use of sapphire. Low resolution X-ray diffraction spectra showed GaN peak positions corresponding to

(0002) and (0004) reflections, suggesting a highly crystalline structure. The films will be further characterized for electrical (Hall, FTIR), optical (PL) and structural (HRXRD) properties.

Increasing the growth temperature to 700°C produced a poorer quality GaN epilayer. Under the Nomarski contrast microscope the surface morphology deteriorated, and X-ray measurement produced peaks of lower intensity than those grown at 650°C. This trend continued when the growth temperature was further increased to 750°C with a complete disintegration of the surface, producing only island-like growth with low X-ray peak intensities confirming a departure from crystallinity. This is a consequence of the above mentioned H_2/Ga reaction at high temperatures. Some of the solutions that are being investigated to eliminate this problem include the growth a buffer layer of III-N at low temperature before depositing the epilayer or growth in a N_2 atmosphere.

In the case of $LiAlO_2$, the temperature change did not affect the uniformity or quality of the layers which grew 3 to 4 times thicker than those on $LiGaO_2$ (Fig. VI.1). X-ray diffraction suggests polycrystalline growth similar to that reported for GaN growth on Si. This can be confirmed by the presence of three almost equally spaced peaks at 32.83°, 34.98° and 37.25° degrees.

The other technology being pursued is the development of the merged-hydride technique for the chemical vapor deposition (CVD) of gallium nitride (GaN). In this technique, a novel chemistry permits the high growth rates of conventional hydride CVD to be achieved using metalorganic sources instead of liquid gallium boats. The advantages of this technique are the abrupt control of dopants and film composition characteristic of metalorganic CVD (MOCVD), which would allow fabrication of electronic and photonic devices several times more quickly than the current leading-edge technology. Furthermore, such high growth rates present the opportunity to grow substrates of GaN. This is a crucial area of research, as all commercially available substrate materials have either thermal expansion mismatches (which leads to stress and possible cracking in the grown film), or lattice parameter mismatches (which leads to poorer crystal quality).

Our group has achieved growth of gallium nitride with the merged-hydride technique at temperatures ranging from 450 to 900°C, and single-crystal growth from 675 to 900°C. Growth rates have varied between 15 and 80 μm/hr, depending upon growth parameters. These values are similar to those of the hydride chemistry, and represent a considerable increase over MOCVD rates, which typically range from 1 to 4 μm/hr. Future work for this project includes continual investigation of process dynamics, and may include such topics as substrate growth, selective epitaxy, doping studies, and device fabrication.

(VII) Development of Diode Lasers (Peter Zory)

II-VI Materials

Using the liquid contact luminescence (LCL) technique described previously in conjunction with modeling, we have

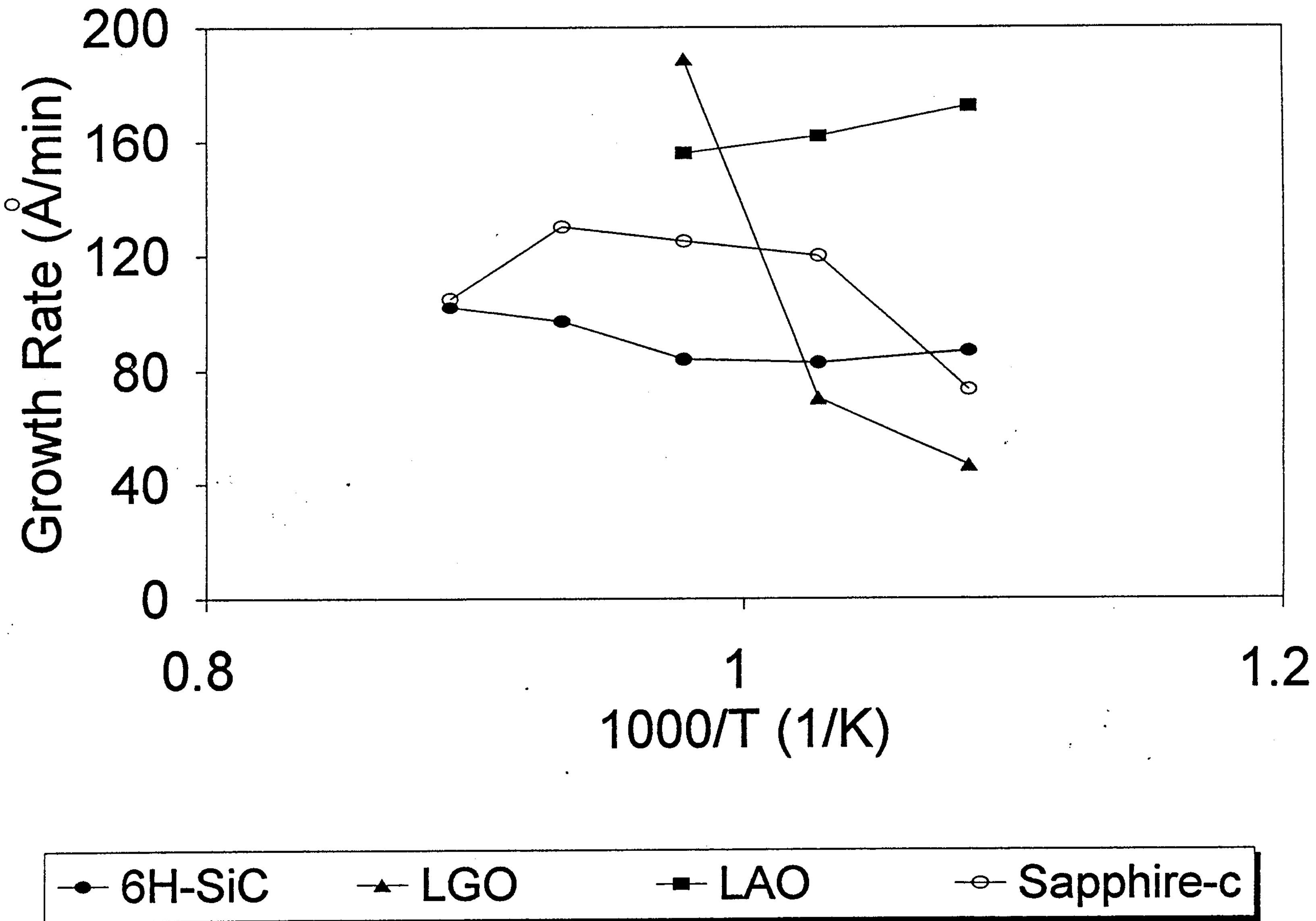

Fig. VI.1.

determined the room temperature, non-radiative lifetime for carriers in CdZnSe and GaAs quantum well (QW) laser material. Values of about 2 ns and 10 ns were obtained for the CdZnSe material(provided by 3M) and GaAs materials, respectively. We are continuing to refine our experiments and modeling in order to improve our confidence in these numbers and to determine the overall utility of the LCL technique for evaluating the quality of CdZnSe diode laser material.

III-V Materials

(1) Work is continuing in the photopumping evaluation of GaN-based materials using the 337 nm nitrogen laser.

(2) Design work has begun on a grating-coupled/distributed feedback, double-heterojunction GaN/AlInN diode laser. The design utilizes a digital metal grating, obviating the need to develop sub-micron GaN etching techniques.

(VIII) Theoretical Calculations of Dopants of ZnSe (Gertrude Neumark)

As given in previous reports, we are able to account for observed activation energies, in relatively lightly doped samples, with "standard" Coulomb screening theory [e.g. G.F. Neumark, Phys. Rev. **B 5**, 402 (1972) and J. Appl. Phys. **48**, 3618 (1977)]. We have now started to investigate more heavily doped samples. Such samples show deep luminescence peaks (at about 2.55 eV), showing a strong peak shift with excitation intensity. This behavior is indicative of potential fluctuations in the sample, caused by random fluctuations in ion concentrations; the fluctuation model is shown in Fig. VIII.1. As can be seen, the situation is complex. We have been able to account for the luminescence features approximately, using reasonable numbers for acceptor concentration and compensation (submitted to J. Cryst. Growth). For fitting to electrical data (hole concentration), an averaging over the fluctuations will be required, and we are presently investigating this aspect.

(IX) MOCVD Growth of GaN (Jacques Pankove)

Our objective is to grow p-n junctions in GaN that will be the basis for short wavelength emitters and lasers. Development of materials for high efficiency LEDs and lasers demands control of optical loss mechanisms such as free carrier absorption and gap state absorption. One technique for probing these gap states is photoconductivity spectroscopy and photoconductivity decay. Work this period has focused on expansion of our previous photoconductivity measurements to study the gap states in GaN. We have measured the photoconductivity decay of several undoped n-type samples grown in our cold-wall MOCVD systems. The decay characteristics of the six samples measured varies only little, while the sample carrier concentrations changed over one order of

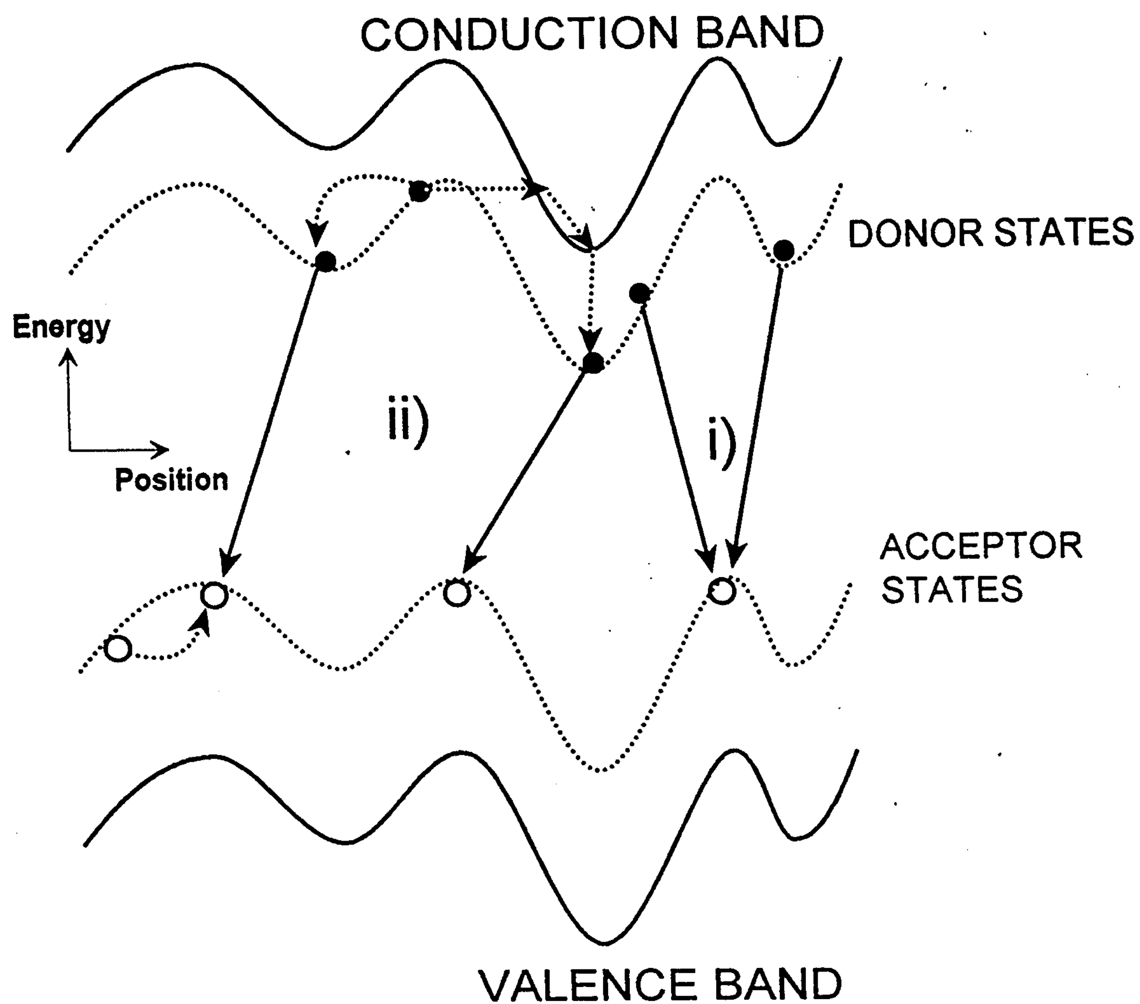

Fig. VIII.1. A schematic representation of the pertubed band and impurity states. Electrons captured at the impurity states recombine with holes at the closest acceptor, leading to "non-vertical" transition (case i). The carriers could also tunnel to the closest well, prior recombination, thus reducing energy of recombination (case ii)).

magnitude. All samples exhibited a power-law dependence at room temperature, decaying as $\sigma_{ph}(t)=At^{-\alpha}$, with α varying by less than a factor of two between samples. No obvious correlation could be made between the α parameter and the electrical characteristics of the films. Fig. IX.1 shows a typical photoconductivity decay response for an n-type sample.

We also measured the temperature dependence of photoconductivity decay for one of the n-type samples. The decay followed a power-law dependence for all temperatures over nearly five decades in time. For temperatures below room temperature, the α parameter was nearly constant, while above room temperature the α parameter increased with temperature, indicating faster non-equilibrium carrier recombination at higher temperatures. Fig. IX.2 shows the dependence of the α parameter on temperature for this sample.

We plan to extend these measurements to include both Mg-doped p-type GaN and higher quality n-type samples.

(X) Gain Modeling in II-VI Strained-Layer QW Structures (Reinhart Engelmann)

Summary

The commercial two-dimensional electronic/optoelectronic device simulation software package (SILVACO) described in our previous report was used to study the lateral behavior of gain-guided II-VI SCH QW laser structures. Both the electrical as well as optical characteristics of such lasers were obtained.

The commercial SILVACO software package directly supports the III-V materials such as the GaAs/AlGaAs and InGaAsP/InP systems for two-dimensional (2-D) electronic and optoelectronic device simulation. We have reported on the simulation of an InGaAsP/InP BH laser diode previously [1]. For the simulation of device structures based on the ZnCdSe/MgZnSSe material system we have incorporated a special input file with relevant material parameters, such as band gap and effective mass.

Based on this input we have simulated the electrical characteristics of a standard ZnCdSe/ZnSSe/MgZnSSe SCH strained QW diode laser with a 10 μm stripe geometry contact at injection levels below threshold. Both radiative and non-radiative recombination is considered. For radiative recombination, the phenomenological bimolecular spontaneous emission model, with a recombination constant B, is used. Non-radiative recombination is described by the Shockley-Read-Hall relation. Stimulated emission and the electronic-optical interaction is neglected for the electrical modeling. Since the software package does not include the Schroedinger equation, QW effects can be included only in a phenomenological way using properly adjusted band gaps and effective masses.

For simulating the lasing characteristics at higher injection levels, the stimulated emission and waveguiding is properly accounted for by using a phenomenological input for the gain relationship (called "empirical" model by SILVACO). The

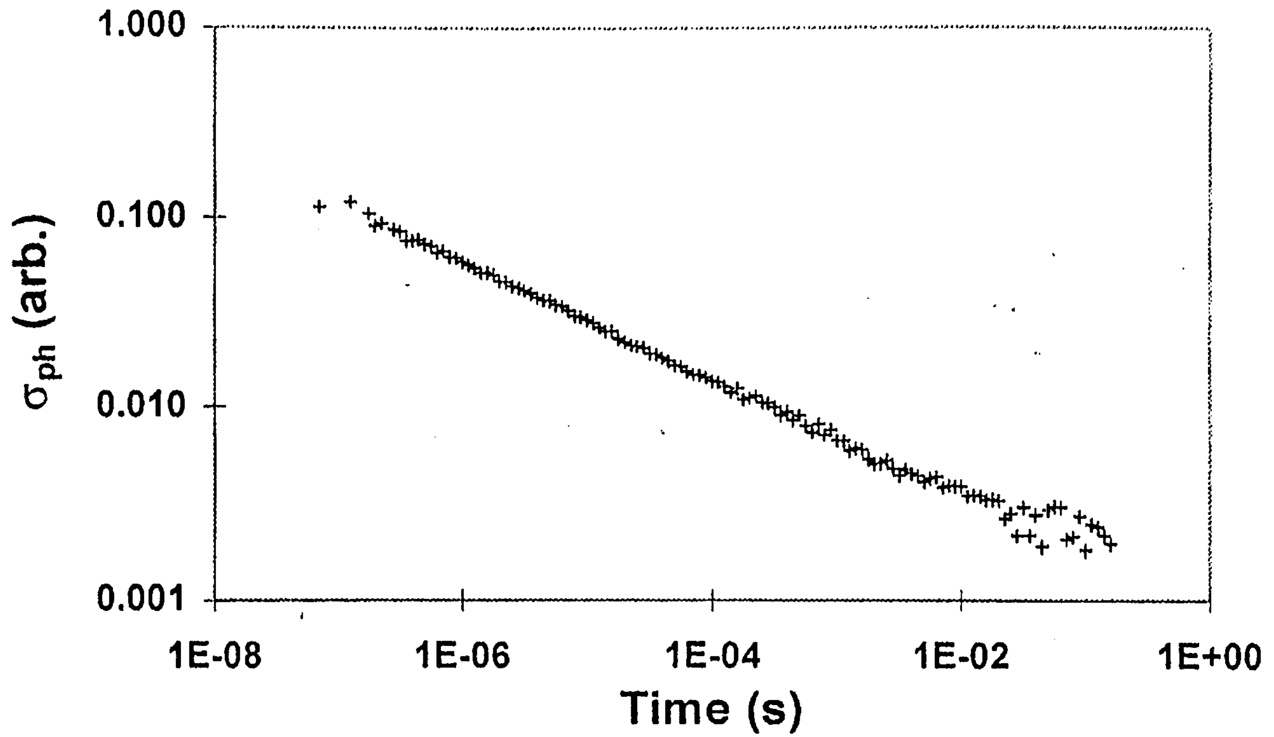

Fig. IX.1. Photoconductivity decay response of n-type GaN sample.

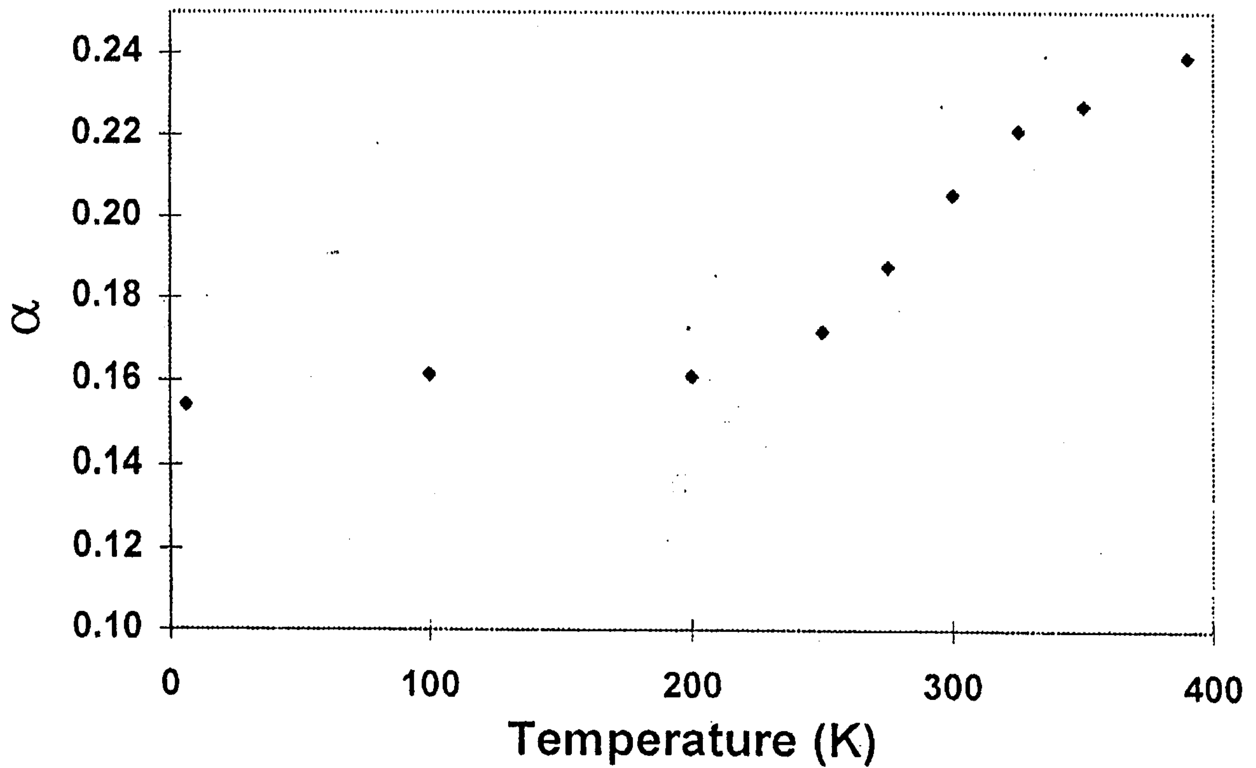

Fig. IX.2. Temperature dependence of α parameter for n-type GaN sample.

coefficients of this latter relationship are adjusted to match the peak gain behavior that we have previously obtained from our one-dimensional (1-D) strained QW model. In a similar way the recombination constant B is chosen from the spontaneous emission results of the 1-D model. A complete two-dimensional simulation of QW diode laser structures is achieved in this way.

The simulations are performed for a 540 μm wide chip of a SCH QW structure with a 10 μm ohmic stripe contact as shown in Fig. X.1. The length of the chip (cavity) is chosen to be 1 mm. The structure consists of a 6.5 nm wide strained $Zn_{0.2}Cd_{0.8}Se$ QW sandwiched between two 100 nm wide $ZnS_{0.06}Se_{0.94}$ barrier layers and 1 um thick $Mg_{0.1}Zn_{0.9}S_{0.14}Se_{0.86}$ claddings. The barrier and cladding layers are lattice-matched to the GaAs substrate. The substrate (including any buffer layer) is assumed to be an ideal n-type ohmic contact to the bottom cladding layer and, hence, is not considered in the simulation. Similarly, special p-contacting layers are neglected and the 10 μm wide contact stripe is assumed to be an ideal ohmic p-contact to the top cladding layer. Both top cladding and barrier layers are doped to a level of 5×10^{17} cm^{-3} acceptors, both bottom cladding and barrier layers to a level of 10^{18} cm^{-3} donors. The QW is considered to be undoped. The pertinent material parameters are summarized in Table 1. The conduction band-offset ratio was assumed to be 0.6. eV Å value of 4 was chosen for the linewidth enhancement factor, a, that governs the antiguiding effect.

Fig. X.2 shows the mesh structure chosen for the simulation. It should be noted that the mesh is most dense in those critical regions where large variations of important physical quantities are expected, particularly at the hetero-boundaries of the QW. The total number of mesh points is 4698 which compares to a maximum available of 4800. All simulations are performed at room temperature (300 K).

The current-voltage characteristic is plotted in Fig. X.3. As expected from the QW band gap (see Table X.1), the turn-on voltage is about 2.5 V. For improved accuracy, stimulated emission and waveguiding was included for bias values above 2.5 V. At three bias values (0, 2.5 and 2.9 V) the vertical profiles of important physical quantities along the stripe center are shown in Figs. X.4 - X.7. Fig. X.4 demonstrates the disappearance of the junction built-in potential in the band diagram as the forward bias is raised from zero to the value of 2.9 V which is close to the actual lasing threshold. Thus, the flat-band condition is indeed established at bias values near threshold, as is widely assumed in one-dimensional (vertical) laser modeling. Note, however, the slight band bendings near the hetero-boundaries caused by the space charges generated from carrier imbalances. The complete vertical carrier distributions are provided in Fig. X.5 along with the impurity doping profile. Already at 2.5 V, a substantial carrier accumulation clearly occurs in the QW. Electrons still outnumber holes because of the stronger electron confinement provided by the chosen band offset ratio (cf. Fig. X.4). Also, considerable minority carrier injection is observed in the barrier layers. Close to lasing threshold, at 2.9 V, the hole concentration in the QW almost reaches that of the electrons indicating the strong

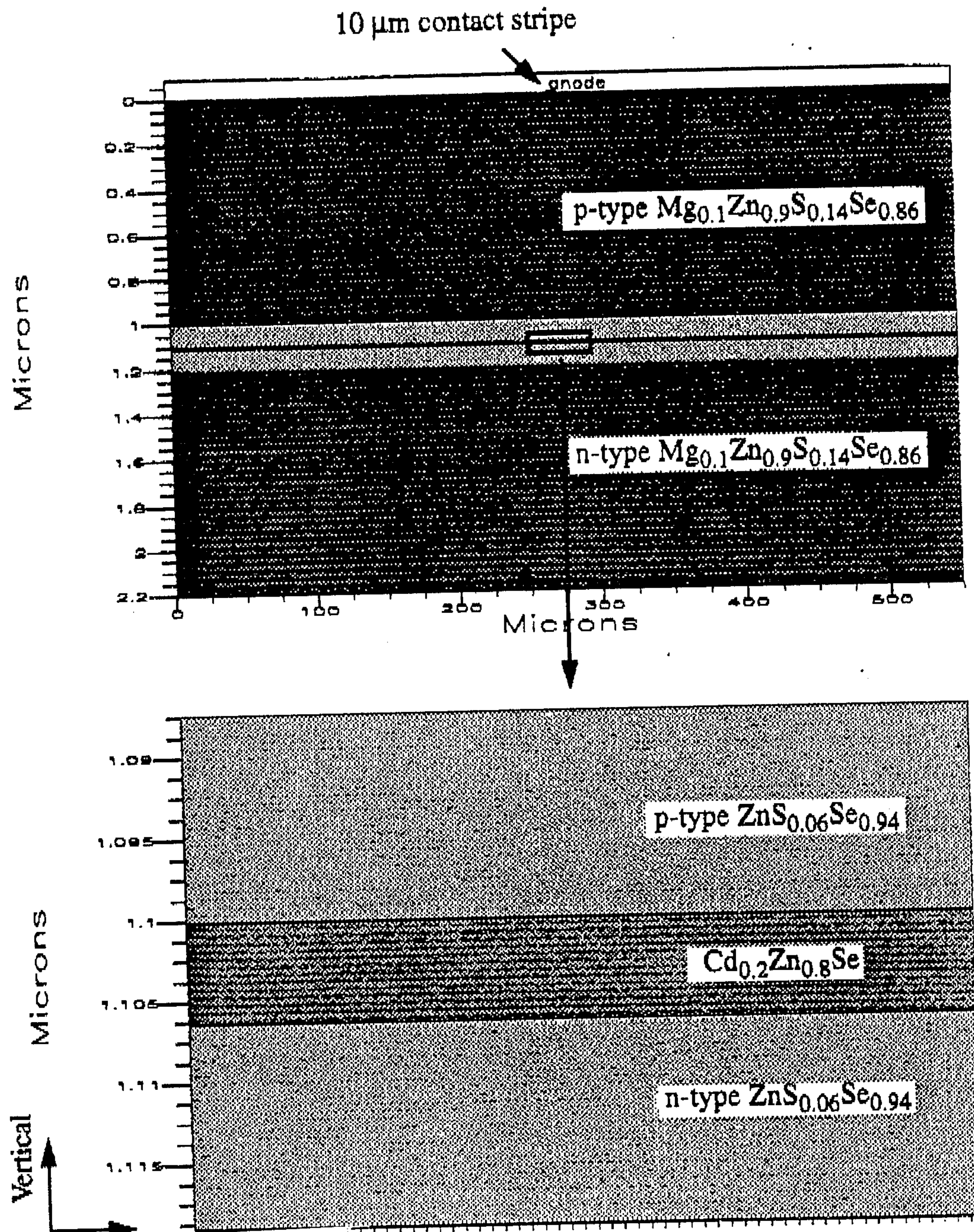

Fig. X.1. $Cd_{0.2}Zn_{0.8}Se/ZnS_{0.06}Se_{0.94}/Mg_{0.1}Zn_{0.9}S_{0.14}Se_{0.86}$SCH QW laser structure cross section (vertical and lateral).

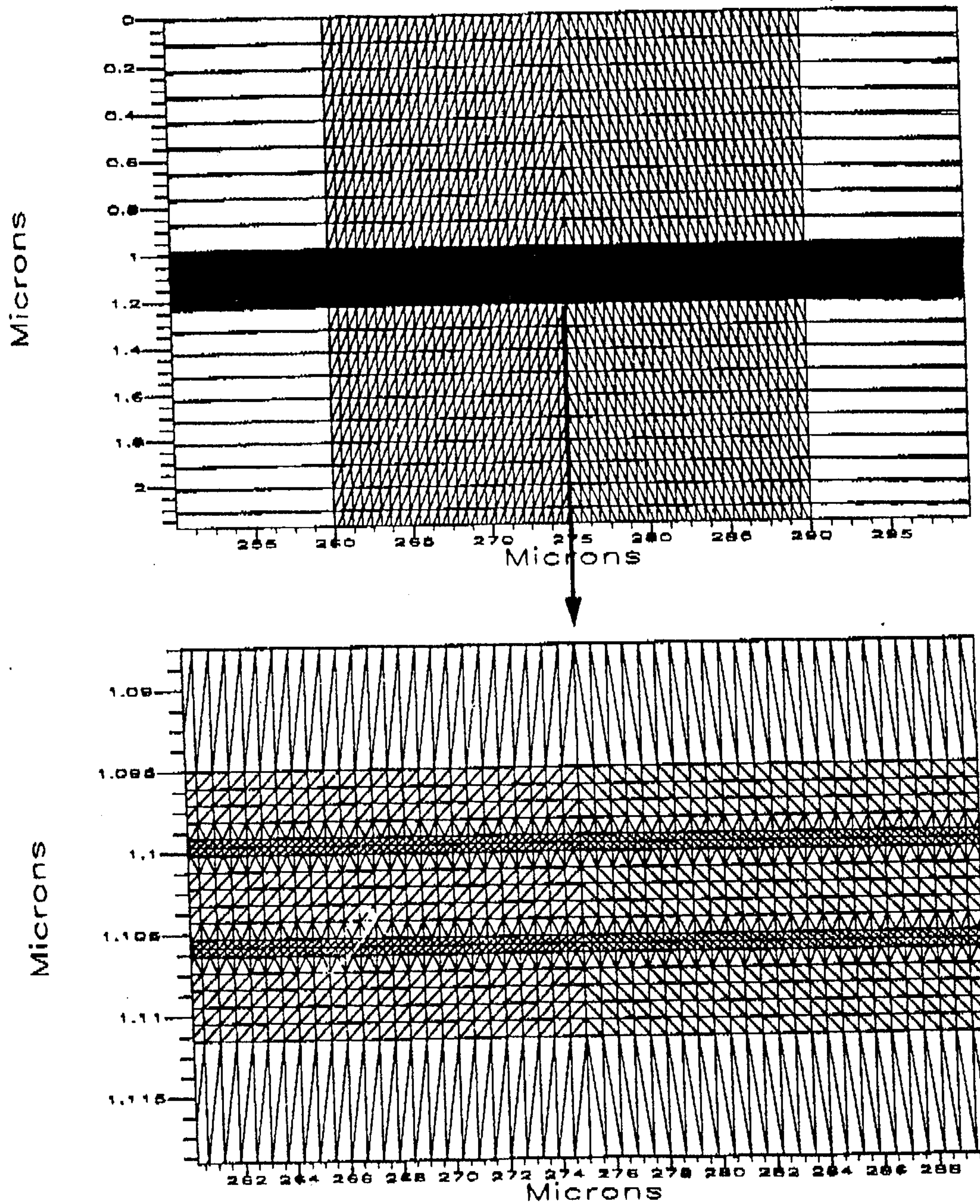

Fig. X.2. Mesh structure for device simulation.

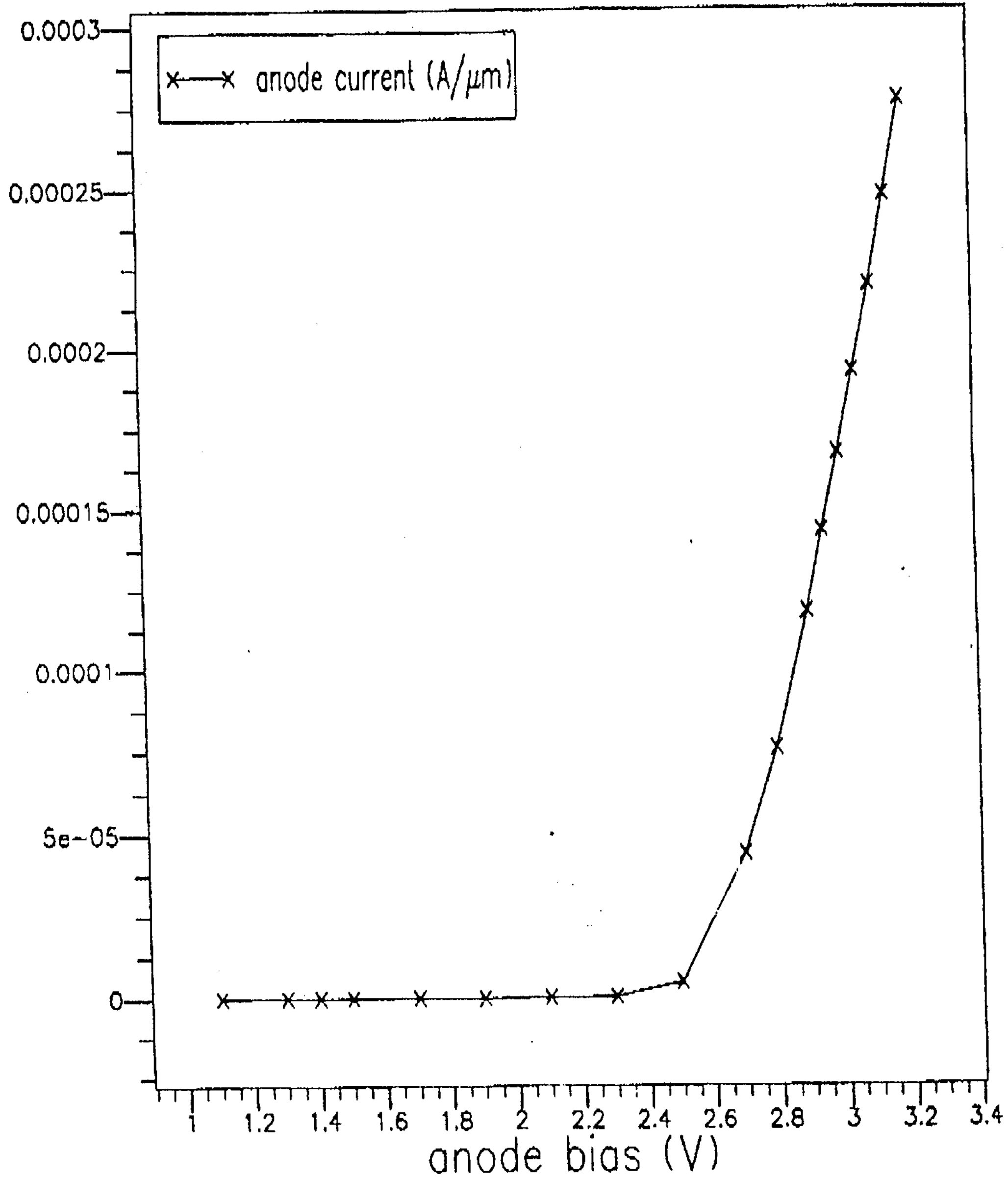

Fig. X.3. Voltage - current relation of CdZnSe/ZnMgSSe SCH QW laser diode. Current normalized to longitudinal dimension (L = 1 mm).

Table X.1. Parameters of ZB CdZnSe/ZnSSe/MgZnSSe Material System @ RT.

	$Cd_{0.2}Zn_{0.8}Se$ Strained QW	ZnSe	$ZnS_{0.06}Se_{0.94}$	$Mg_{0.1}Zn_{0.9}S_{0.14}Se_{0.86}$
a (Å)	5.744	5.668	5.652	5.652
E_g (eV)	2.46	2.70	2.73	2.85
m_e (m_0)	0.140	0.149	0.149	0.18
m_{hh} (m_0)	0.18, 1.16	0.57	0.6	0.61
m_{lh} (m_0)	0.32, 0.14		0.23	
γ_1	4.3	4.3	4.3	
γ_2	1.14	1.14	1.14	
γ_3	1.84	1.84	1.84	
C_{11} (N/m^2)	8.42×10^{10}	9.0×10^{10}	9.04×10^{10}	
C_{22} (N/m^2)	5.26×10^{10}	5.34×10^{10}	5.34×10^{10}	
C_{44} (N/m^2)	3.88×10^{10}	3.96×10^{10}	3.69×10^{10}	
a_v (eV)	-5.04	-5.82	-5.82	
b_v (eV)	-1.12	-1.2	-1.2	
μ_e (cm^2/Vs)	600	500	479	250
μ_{hh} (cm^2/Vs)	60	30	66	10
ε_0	10.6	7.6	8.5	
ε_∞	8.2	5.4	5.3	
n (@500nm)	2.88	2.8	2.74	2.62
E_A (meV)		100 (N)	100 (N)	110 (N)
E_D (meV)		20 (Cl)	20 (Cl)	20 (Cl)

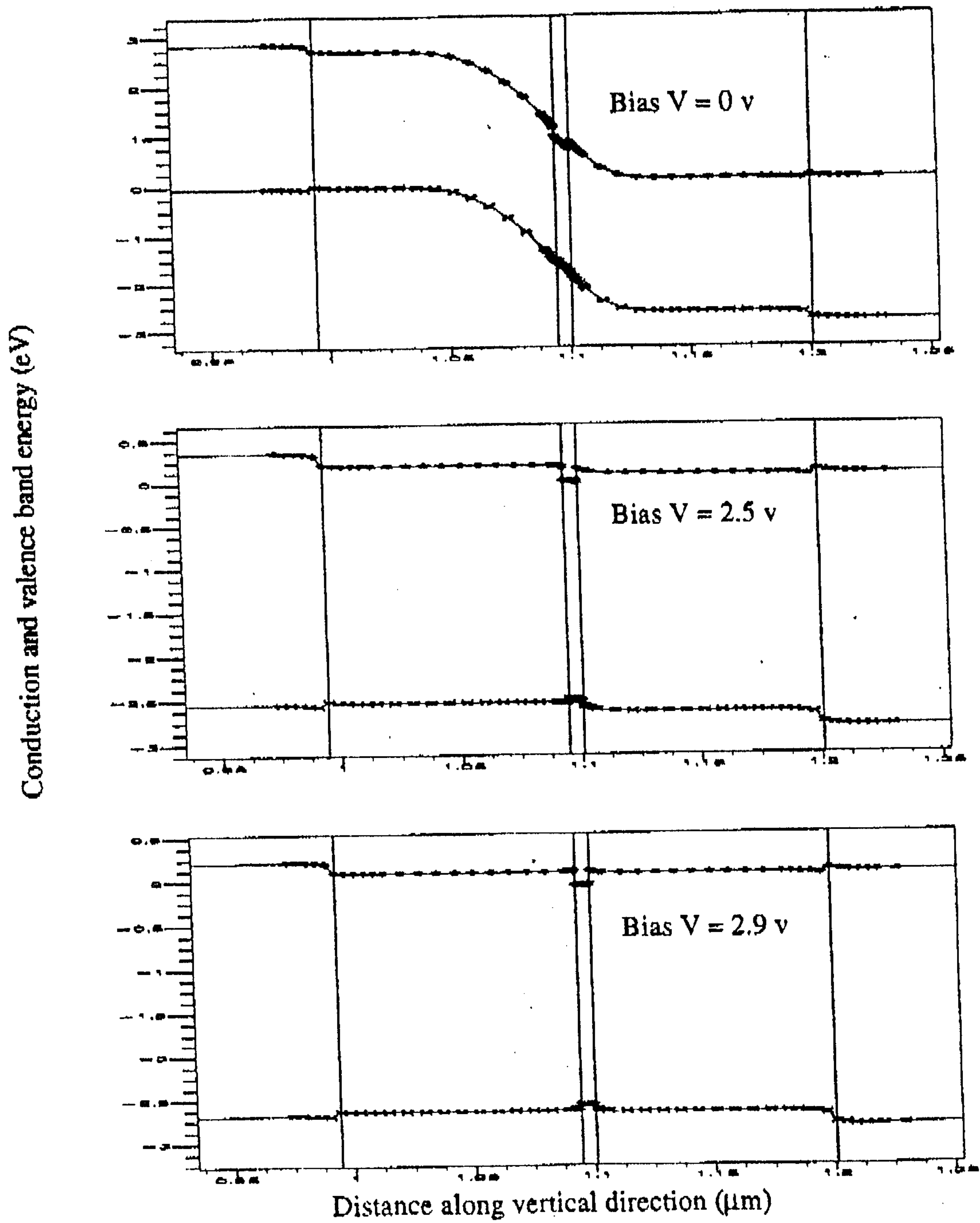

Fig. X.4. Band diagram under different bias voltages.

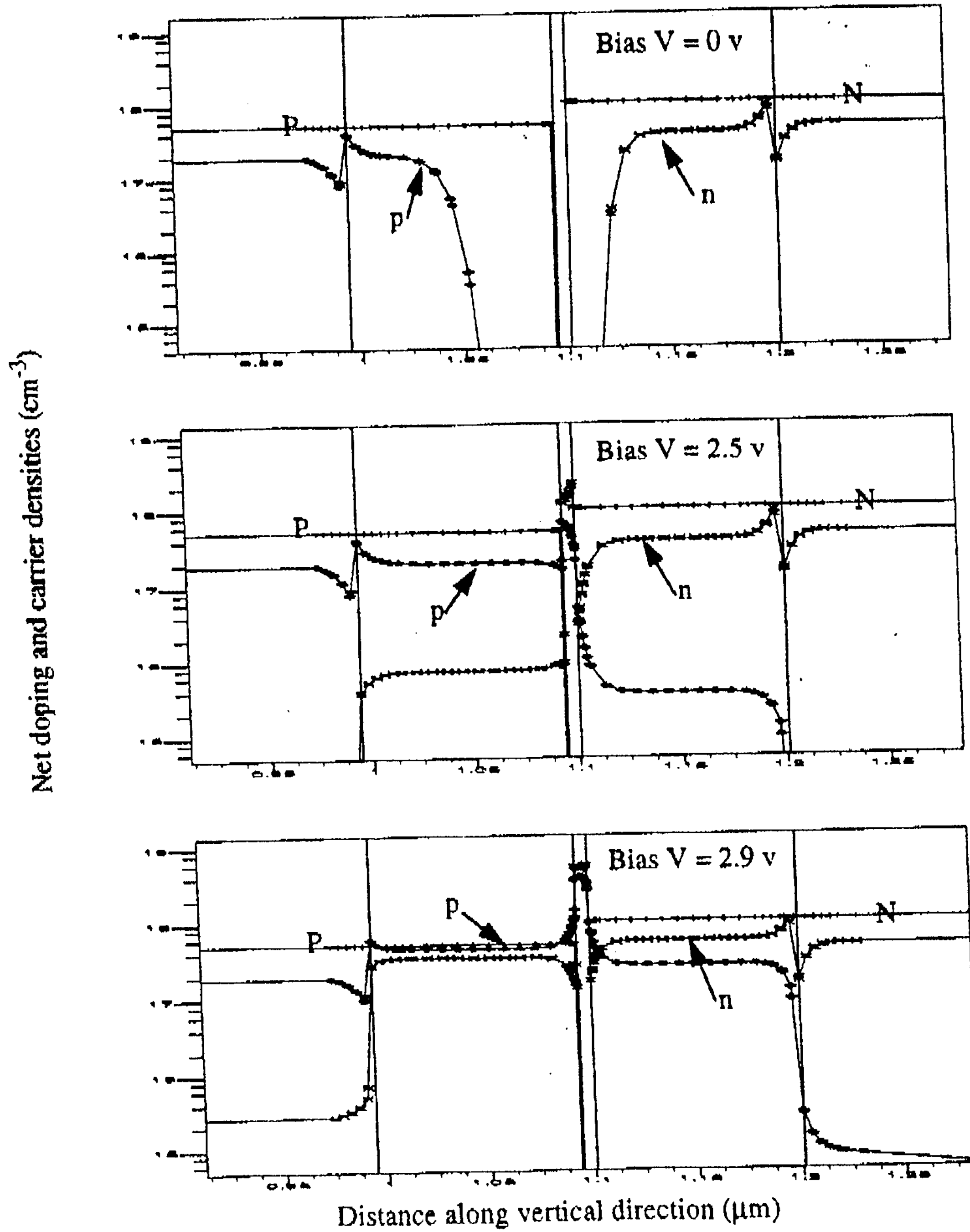

Fig. X.5. Net doping profile and carrier concentrations.

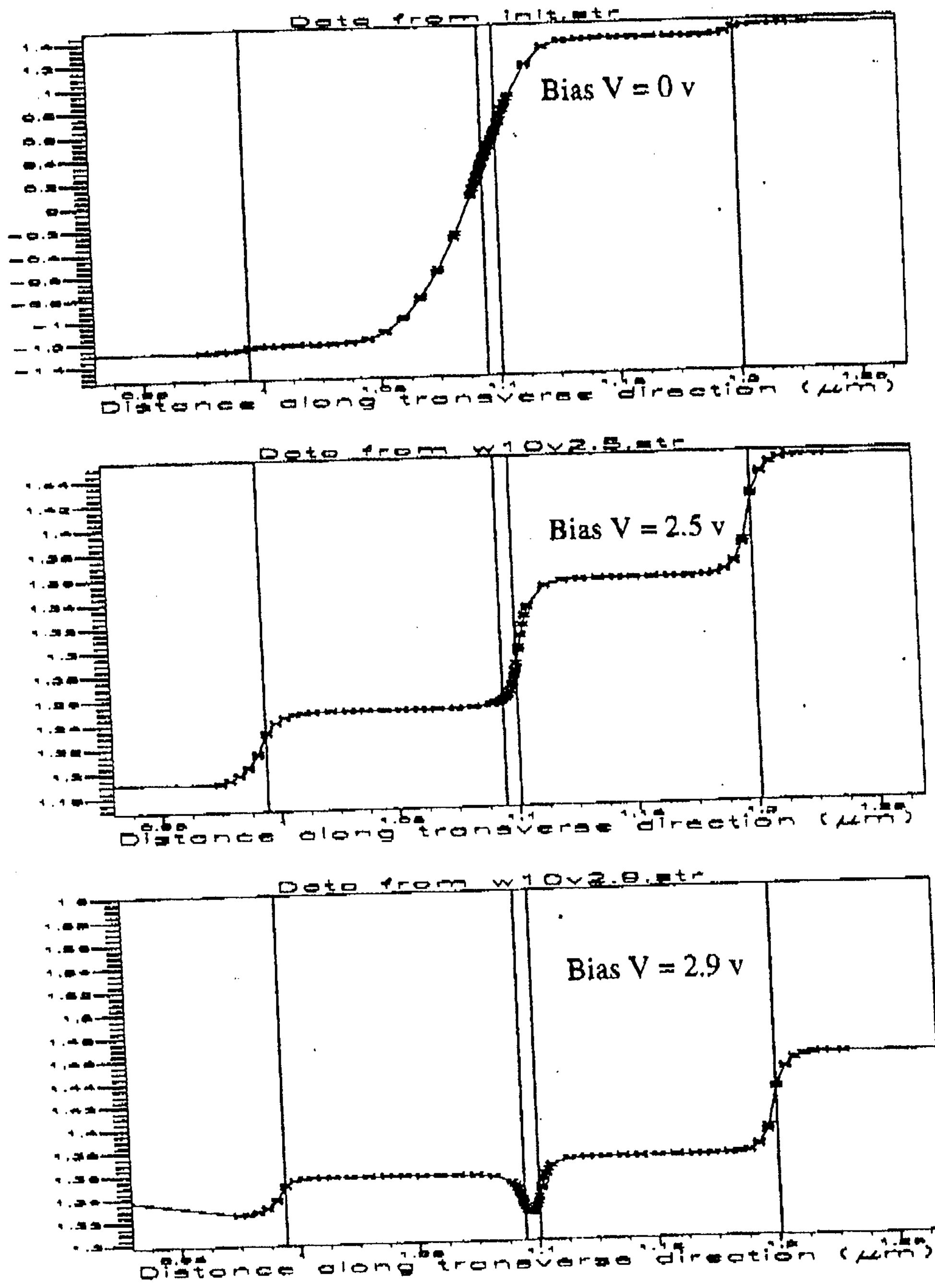

Fig. X.6. Potential distribution along vertical direction.

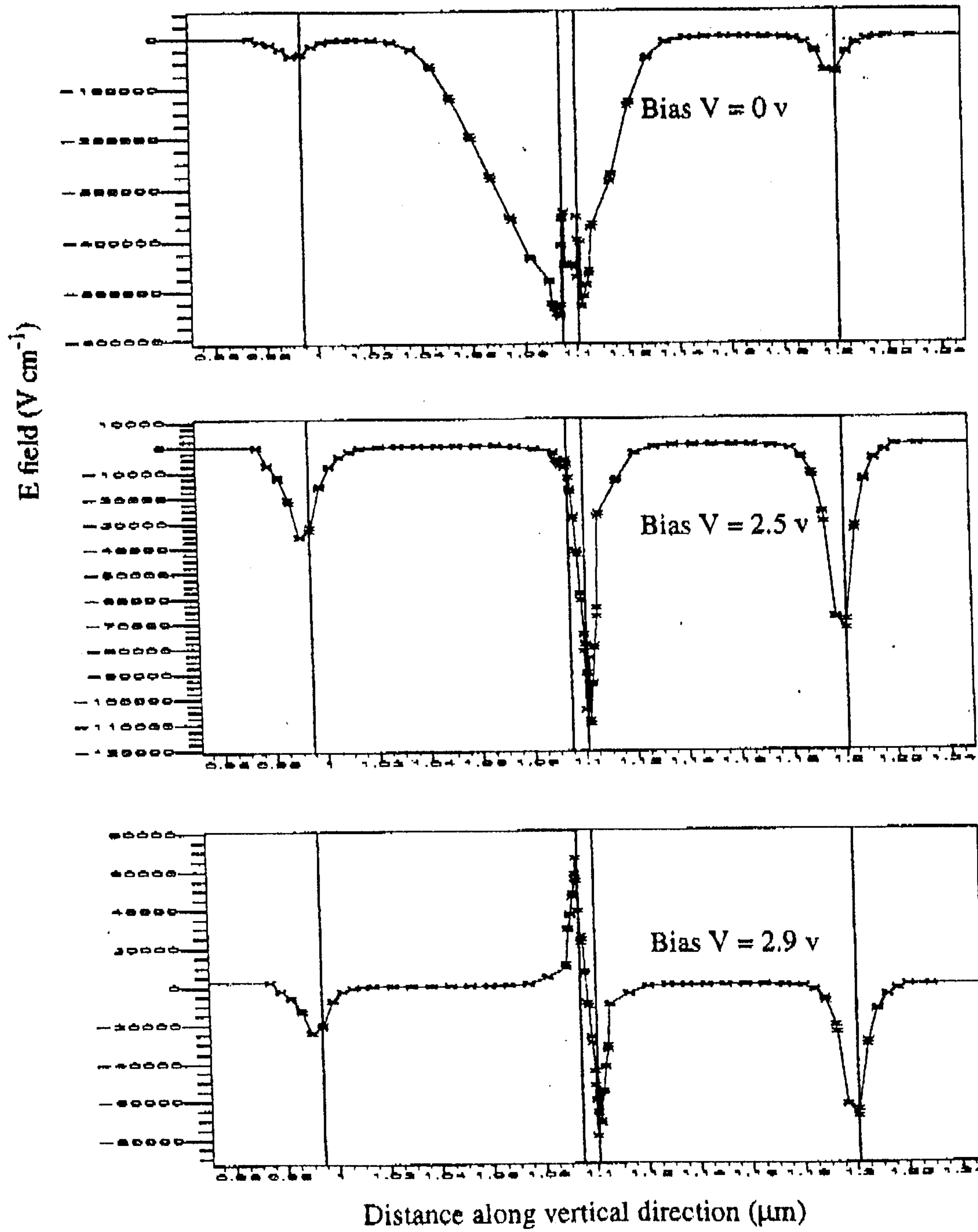

Fig. X.7. Vertical-transverse electrical field distribution.

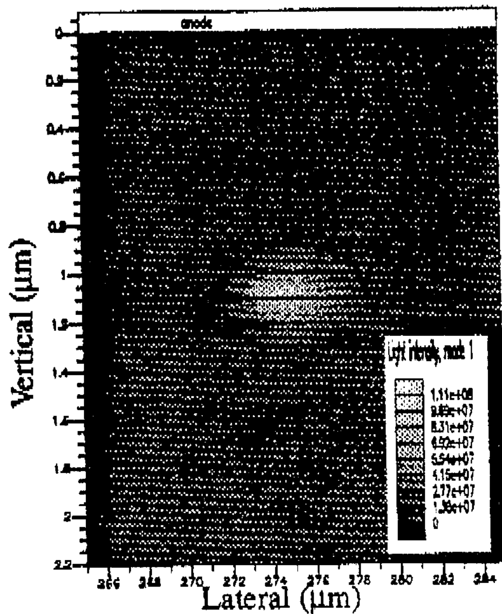

(a) Near field pattern at 3.2 V

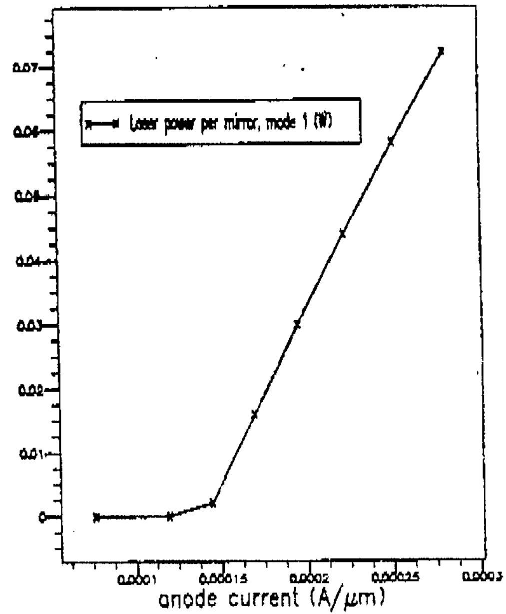

(b) L - I relation

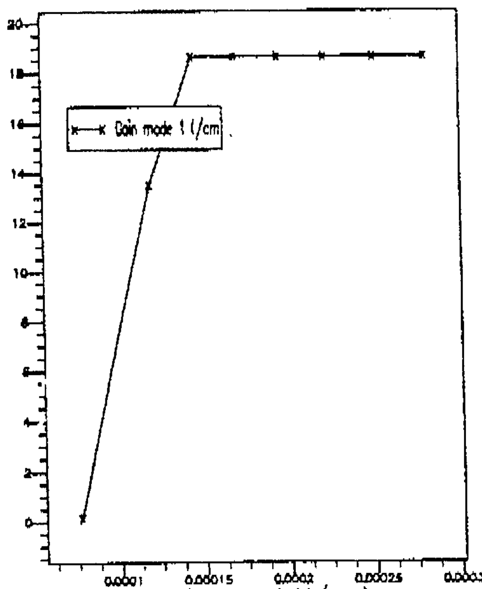

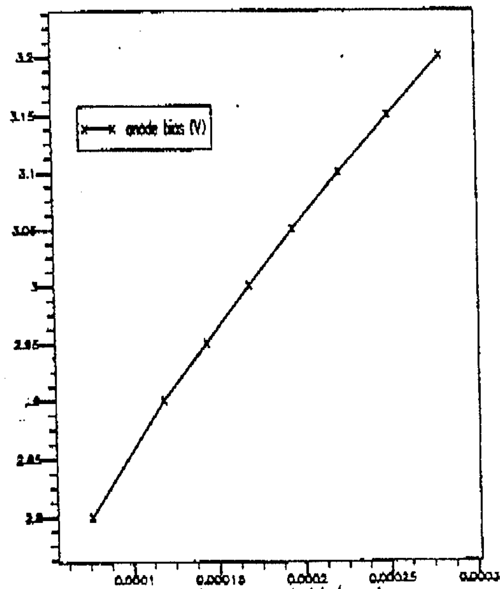

Fig. X.8. 2-D simulation results of gain guided 10 μm strip QW laser Current is normalized to the longitudinal dimension (cavity length L = 1 mm).

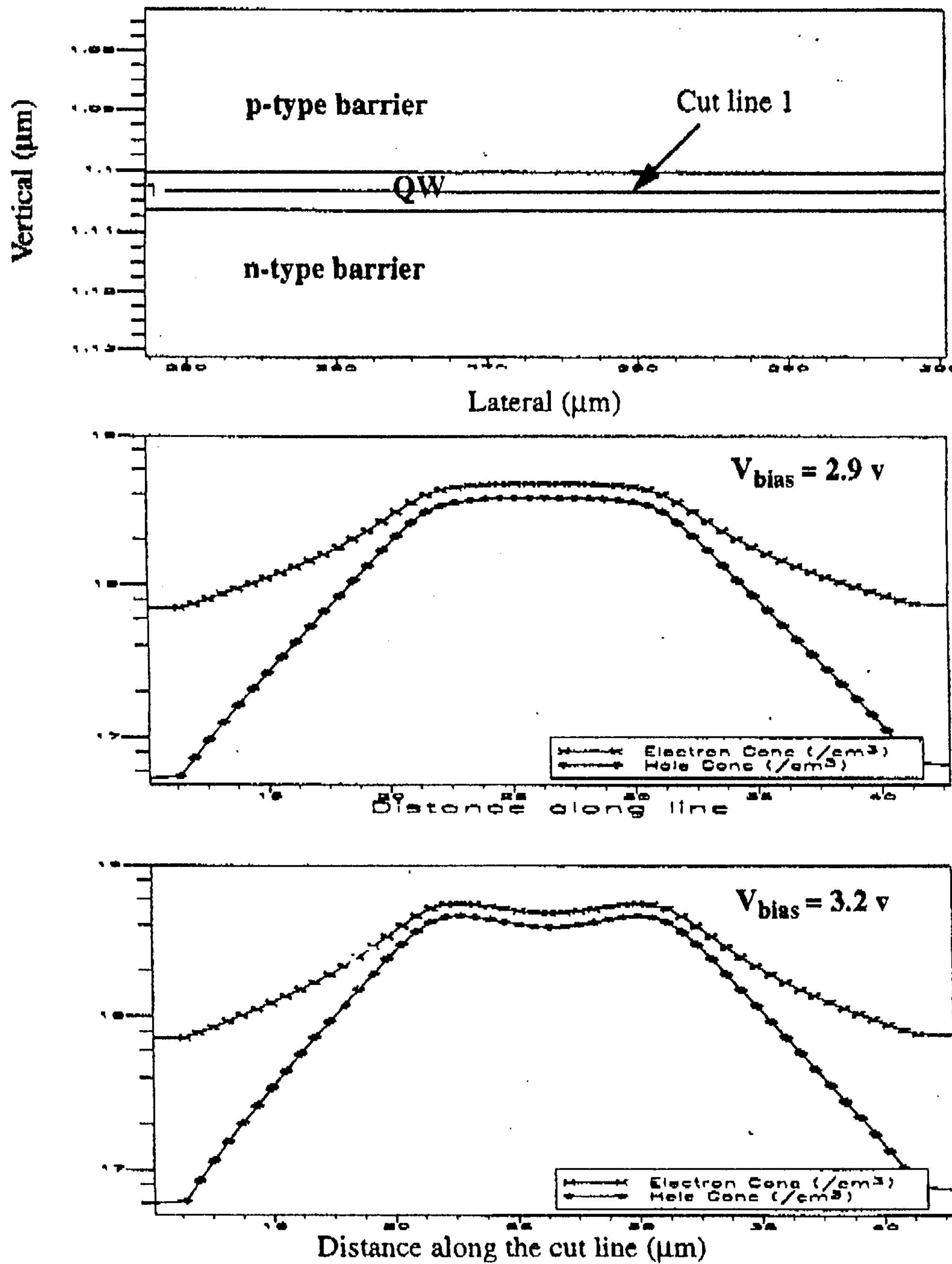

Fig. X.9. lateral carrier density distribution of gain guided 10 μm strip QW laser.

electrostatic hole-confinement effect of the negative electron space charge; in addition, the minority carrier injection into the barriers has increased dramatically. Even some minority carrier injection into the cladding layers is now observed. Carrier injection into the barrier and cladding layers, of course, contributes to an undesirable diode leakage current.

Figs. X.6 and X.7 show the electrical potential and field profiles, respectively. Fig. X.6, at 2.9 V bias, clearly demonstrates the electrostatic hole confining effect in the QW caused by the stronger electron accumulation in this region. A field built-up in the lower-resistivity p-cladding layer is also seen. It is interesting to note that the charge imbalance near the hetero-boundaries leads to dramatic field spikes generating peak values as high as 110 kV/cm (Fig. X.7, bias 2.5 V, at the n-side QW hetero-boundary). Effects caused by possible field ionization in these field spikes remain speculative and are, of course, not considered in the modeling program.

The simulation in the lasing regime was performed for a single frequency only (single spatial resonance mode). The results for the zero-order lateral mode at the longitudinal resonance of 500 nm (1 mm cavity length) are summarized in Fig. X.8. It is interesting to note that care had to be taken in setting up the simulation in order to produce the zero order lateral mode. When starting the simulation from the lateral chip edges, invariably a higher-order solution was obtained with a higher lasing threshold. In order to achieve the zero-order mode solution the simulation procedure had to be confined to the region close under the stripe. It is believed that the inherent instabilities of gain guiding coupled with the "numerical noise" of the simulation tend to produce such a behavior.

Fig. X.8a provides a mode pattern above threshold. The lateral mode width (FWHM) is about 5 μm and is the result of strong positive guiding generated by spatial hole burning as demonstrated by the lateral carrier profiles shown in Fig. X.9. The light output vs. current characteristic is plotted in Fig. X.8b, showing a threshold current of about 137 mA which translates to a threshold current density of about 1.4 A/cm^2 if normalized to the contact stripe area. This relatively large value is obviously caused by the lateral current spreading and the non-radiative and leakage current components accounted for in the model. Gain clamping at threshold is demonstrated in Fig. X.8c. Fig. X.8d shows the eventual expanded current-voltage characteristic (a section of Fig. X.3).

We plan to apply the 2-D modeling procedure for additional simulations of blue-green II-VI laser structures, particularly for investigating the influence of the stripe width on the laser performance. Further plans relate to analyzing the band gap structure of cubic GaN and InN for modeling an InGaN laser and to the influence of potential impurity banding on device performance.

Thesis

- Austin C. Frenkel, M.S. Degree, Aug. '95, "Growth by rf plasma-MBE and in-situ characterization of InN and InGaN thin films."

Papers this quarter

- C.M. Rouleau, C.J. Santana, K.S. Jones and R.M. Park, "Dislocations in lattice-mismatched wide-gap II-VI/GaAs heterostructures as laser light scatterers: Experiment and theory," J. Appl. Phys. 78, 1203 (1995).

- C. Kothandaraman, G.F. Neumark, and R.M. Park, "Compensation in heavily N-doped ZnSe: A luminescence study", submitted to J. Cryst. Growth.

- The PHYSICS TODAY article, "Blue-green diode lasers", by G.F. Neumark, R.M. Park, and J.M. DePuydt, has been reprinted, as the cover story, by the Japanese magazine PARITY, after translation into Japanese.

Presentations this quarter

- In conjunction with the IEEE/LEOS Distinguished Lecturer Award, Peter Zory gave a colloquia on blue-green diode lasers at six universities in Australia.

- I. Kuskovskiy, and G.F. Neumark, "Characterization of ZnSe:N using screening effects," submitted to 1995 Fall MRS Meeting.

- C. Kothandaraman, G.F. Neumark, and R.M. Park, "Compensation in heavily N-doped ZnSe: A luminescence study," Seventh Intl. II-VI Conference, Edinbrough, Scotland, Aug.1995.

- R.M. Park, "Development of wide-gap II-VI materials for blue-green diode laser applications: A review," paper presented at the National Science Foundation (NSF) Forum on Optical Science and Engineering, part of SPIE's 1995 International Symposium on Optical Science, Engineering and Instrumentation, 9-14 July 1995, San Diego, CA - Invited. (To be published in SPIE Proceedings Volume 2524).

- R.A. Taylor, R.A. Adams, J.F. Ryan and R.M. Park, "Time-resolved exciton dynamics and stimulated emission from ZnCdSe/ZnSe multiple quantum well structures," Seventh International Conference on Modulated Semiconductor Structures, July 10-14, Madrid, Spain.

- R.A. Taylor, R.A. Adams, J.F. Ryan and R.M. Park, "Exciton recombination dynamics in ZnCdSe/ZnSe quantum wells." Seventh International Conference on II-VI Compounds and Devices, August 13-18, 1995, Edinburgh, Scotland.

Presentations this quarter [Continued]

- J.T. Trexler, J.J. Fijol, L.C. Calhoun, R.M. Park and P.H. Holloway, "Electrical contacts to p-ZnTe." Seventh International Conference on II-VI Compounds and Devices, August 13-18, 1995, Edinburgh, Scotland.
- Li Wang, J. Simmons, M. Jeon and R.M. Park, "Exciton Dynamics in CdZnSe/ZnSe multiple quantum wells," 37th Electronic Materials Conference, June 21-23, 1995, Charlottesville, VA.
- Paul H. Holloway, "Surface Analysis of Solids," Summer Institute at University of Helsinki, Aug. 7-11, 1995, Helsinki, Finland.

REFERENCES

[1] C.R. Abernathy, J.D. MacKenzie, S.R. Bharatan, K.S. Jones, and S.J. Pearton, Appl. Phys. Lett. **66**, 1632 (1995).

[2] R.J. Molnar and T.D. Moustkas, J. appl. Phys. **76**, 4587 (1994).

[3] Tansley and Egan, Phys. **B 185** (1993) 190.

[4] T.C. Fu, N. Newman, E. Jones, J.S. Chan, X. Liu, M.D. Rubin, N.W. Cheung, and E.R. Weber, J. Elect. Mat., **24**, 249 (1995).

[5] R.C. Powell, N.E. Lee, and J.E. Greene, Appl. Phys. Lett. **60**, 2505 (1992).

[6] M.E. Lin, B. Sverdlov, G.L. Zhou, and H. Morkoc, Appl. Phys. Lett., **62**, 3479 (1993).

[7] A.L. Holmes, K.G. Fertitta, F.J. Ciuba and R.D. Dupuis, Elect. Lett., **30**, (1994).

[8] W.E. Plano, J.S. Major, Jr., D.F. Welch and J. Speirs, Elect. Lett., **30**, 2079 (1994).

Post Doctoral Associates, Graduate Research Assistants, and Undergraduate Research Assistants:

Post Doctoral Associates:

Akhter Ahmed with Dr. Anderson
Ziad Osman with Dr. Anderson
Viswanath Krishnamoorthy with Dr. Jones
Chang-hua Qiu with Dr. Pankove

Graduate Research Assistants:

Bruce Liu with Dr. Park
Minhyon Jeon with Dr. Park

Graduate Research Assistants: (Continued)

George Kim with Dr. Park
K.N. Lee Dr. Abernathy
Jin Hong with Dr. Pearton
Jeff Hsu with Dr. Zory
Jason O. with Dr. Zory
Igor Kuskovskiy with Dr. Neumark
Li Wang with Dr. Simmons
Y. Cai with Dr. Engelmann
William A. Melton with Dr. Pankove
John Fijol with Dr. Holloway
T.J. Kim with Dr. Holloway
Jeff Trexler with Dr. Holloway
Eric Bretschneider with Dr. Anderson
Joe Cho with Dr. Anderson
Todd Dan with Dr. Anderson
J. Kim with Dr. Jones
S. Bharatan with Dr. Jones
S. Bhendi with Dr. Jones

Undergraduate Research Assistants:

Julie Sauer with Dr. Simmons
Bob Covington with Dr. Anderson
Michael Mui with Dr. Anderson
Brendon Cornwell with Dr. Anderson

f:qprdoc.008